DEVELOPMENT OF CLINOPTILOLITE/POLY ε-CAPROLACTONE -POLY ETHYLENE GLYCOL - POLY ε-CAPROLACTONE TRIBLOCK COPOLYMER BASED SCAFFOLDS FOR BONE TISSUE ENGINEERING

A THESIS SUBMITTED TO
THE GRADUATE SCHOOL OF NATURAL AND APPLIED SCIENCES
OF
MIDDLE EAST TECHNICAL UNIVERSITY

BY

AHMET ENGİN PAZARÇEVİREN

IN PARTIAL FULFILLMENT OF THE REQUIREMENTS
FOR
THE DEGREE OF MASTER OF SCIENCE
IN
ENGINEERING SCIENCES

AUGUST 2016

Approval of the thesis:

DEVELOPMENT OF CLINOPTILOLITE/POLY ε-CAPROLACTONE - POLY ETHYLENE GLYCOL - POLY ε-CAPROLACTONE TRIBLOCK COPOLYMER BASED SCAFFOLDS FOR BONE TISSUE ENGINEERING

submitted by **AHMET ENGİN PAZARÇEVİREN** in partial fulfillment of the requirements for the degree of **Master of Science in Department of Engineering Sciences, Middle East Technical University** by,

Prof. Dr. Gülbin Dural Ünver _____
Dean, Graduate School of **Natural and Applied Sciences**

Prof. Dr. Murat Dicleli _____
Head of Department, **Engineering Sciences**

Assoc. Prof. Dr. Ayşen Tezcaner _____
Supervisor, **Engineering Sciences Dept., METU**

Assoc. Prof. Dr. Dilek Keskin _____
Co-supervisor**, Engineering Sciences Dept., METU**

Examining Committee Members:

Assoc. Dr. Senih Gürses _____
Engineering Sciences Dept., METU

Assoc. Prof. Dr. Ayşen Tezcaner _____
Engineering Sciences Dept., METU

Prof. Dr. Caner Durucan _____
Metallurgical and Materials Engineering Dept., METU

Assoc. Prof. Dr. Can Özen _____
Biotechnology Dept, METU

Assoc. Prof. Dr. Pınar Yılgör Huri _____
Biomedical Engineering Dept., Ankara University

Date: 05/08/2016

I hereby declare that all information in this document has been obtained and presented in accordance with academic rules and ethical conduct. I also declare that, as required by these rules and conduct, I have fully cited and referenced all material and results that are not original to this document.

Name, Last Name: Ahmet Engin Pazarçeviren

Signature:

ABSTRACT

DEVELOPMENT OF CLINOPTILOLITE/POLY ε-CAPROLACTONE -POLY ETHYLENE GLYCOL - POLY ε-CAPROLACTONE TRIBLOCK COPOLYMER BASED SCAFFOLDS FOR BONE TISSUE ENGINEERING

Pazarçeviren, Ahmet Engin
M.S., Department of Engineering Sciences
Supervisor: Assoc. Prof. Dr. Ayşen Tezcaner
Co-Supervisor: Assoc. Prof. Dr. Dilek Keskin

August 2016, 89 pages

Bone tissue engineering mainly depends on the feasible substitutes with ability to regenerate damaged bone tissue. One of the applications in which bone tissue engineering mainly focuses on is the production of bone tissue scaffolds. These scaffolds are expected to be biocompatible, highly interconnective and porous to provide a niche for colonizing bone cells. In addition, bone tissue scaffolds should be mechanically strong enough to accommodate compression. Scaffolds should also be biodegradable to encourage bone cell growth and mineralization in order to accomplish bone regeneration at the defect site. Considering the aforementioned, poly (caprolactone) - poly (ethylene glycol) - poly (caprolactone) (PCL-PEG-PCL) triblock copolymer composite scaffolds with clinoptilolite earth mineral were fabricated to provide mechanical strength as well as stable environment for bone tissue growth at the defect site. Clinoptilolite, a natural zeolite, was selected as a bioactive ceramic component for improving tmechanical and biological properties of PCL-PEG-PCL based scaffolds. Highly porous clinoptilolite/poly(ε-caprolactone)-poly(ethylene glycol)-poly(ε-caprolactone) (CLN/PCEC) composite scaffolds with different clinoptilolite contents (10% and 20%) were fabricated with reproducible solvent free powder compression/particulate leaching technique. The scaffolds had interconnective pores and the porosity ranged between 55% to 76%.

CLN/PCEC scaffolds showed negligible degradation within 8 weeks and displayed less water uptake and higher bioactivity than PCEC scaffolds. Presence of clinoptilolite improved the mechanical properties. Highest compressive strength (5.60 MPa) and modulus (114.84 MPa) were reached with scaffold group containing 20% CLN. In vitro protein adsorption capacity of these scaffolds (0.95 mg protein/g scaffold) was also higher for CLN/PCEC scaffolds. They also had higher osteoinductivity in terms of enhanced ALP, OSP activities and intracellular calcium deposition of seeded cells. Stoichiometric apatite deposition (Ca/P=1.686) was observed during cell proliferation analysis with human fetal osteoblasts cells. Thus, it can be suggested that CLN/PCEC composite scaffolds could be promising carriers for enhancement of bone regeneration in bone tissue engineering applications.

Keywords: Clinoptilolite, Amphiphilic copolymer, Particulate leaching, Solvent Free bone scaffolding, Powder compression

ÖZ

KEMİK DOU MÜHENDİSLİĞİ İÇİN KLİNOPTİLOLİT/POLİ ε-KAPROLAKTON – POLİ ETİLEN GLİKOL – POLİ ε-KAPROLAKTON TRİBLOK KOPOLİMER TABANLI HÜCRE TAŞIYICILARININ GELİŞTİRİLMESİ

Pazarçeviren, Ahmet Engin
Yüksek Lisans, Mühendislik Bilimleri Bölümü
Tez Yöneticisi : Doç. Dr. Ayşen Tezcaner
Ortak Tez Yöneticisi: Doç. Dr. Dilek Keskin

Ağustos 2016, 89 sayfa

Kemik doku mühendisliği, zarar görmüş kemik dokusunun yenilenmesini sağlamak amacıyla uygulanabilir ürünler dizaynına dayanmaktadır. Kemik doku mühendisliğinde kullanılan bu kolonizasyonu ve gelişimini teşvik etmek amacıyla biyouyumlu ve yüksek oranda birbiriyle bağlantılı gözenekliliğe sahip olmalıdır. Buna ilave olarak, kemik dokusu iskeleleri kemik tarafından uygulanacak sıkıştırmaya karşı mekanik olarak güçlü olmalıdır. İskeleler aynı zamanda biyobozunur olmalıdır ki bu sayede kemik hücrelerinin gelişimi ve mineralizasyonu engellenmeden yeni kemik dokusunun oluşumu sağlanmalıdır. Bu özellikler göz önünde bulundurularak, poli (kaprolakton) - poli (etilen glikol) - poli (kaprolakton) (PCL-PEG-PCL) triblok kopolimer kompozit iskeleleri bir toprak minerali olan klinoptilolit ile üretilerek zarar görmüş bölgedeki kemik gelişimi için gerekli mekanik gücü ve uygun ortamı sağlaması amacıyla tasarlanmıştır. Taşıyıcıların mekanik ve biyolojik özelliklerinin güçlendirilmesi için doğal bir zeolite olan biyoaktif klinoptilolit seramiği seçilmiştir. Yüksek gözenekliliğe sahip olan klinoptilolit/poli(ε-kaprolactone)-poli(etilen glikol)-poli(ε-kaprolactone) (CLN/PCEC) farklı klinoptilolit oranlarını (%10 ve %20) içerek şekilde tekrarlanabilir çözücü içermeyen toz sıkıştırma/parçacık uzaklaştırma metodu ile üretilmiştir. Bu taşıyıcılar %55 ve %76 arasında değişen birbiriyle bağlantılı gözenekliliğe sahip olduğu bulunmuştur CLN/PCEC taşıyıcıları PCEC taşıyıcılarına oranla daha düşük su ile şişme ve 8 haftalık periyotta yok denecek kadar az bozunma göstermiştir. Taşıyıcılara klinoptilolit eklenmesi mekanik özellikleri.nin arttığı

gözlenmiştir En yüksek maksimum sıkışma kuvvetine (5.60 MPa) ve sıkışma modülüne (114.84 MPa) %20 klinoptilolit içeren taşıyıcı ile ulaşılmıştır. Aynı zamanda en yüksek protein adzorbasyonuna (0.95 mg/g taşıyıcı) en fazla klinoptilolit içeren taşıyıcı ile ulaşılmıştır. CLN/PCEC hücre taşıyıcıları üstlerine ekilen ve etkileştirilen hücreler ile daha yüksek osteoindüksiyon gösterdikleri ALP, OSP aktivileri ve hücre içi kalsiyum birikimi analizleri ile tespit edilmiştir. Buna ek olarak, insan kökenli fetal osteoblast hücreleri ile yapılan çoğalma analizi esnasında tam oranlı apatit birikimi (Ca/P=1.686) gözlemlenmiştir. Dolayısıyla, CLN/PCEC kompozit hücre taşıyıcılarının kemik yenilenme oranını geliştirme potansiyeline sahip olduğu ve bu yüzden de kemik doku mühendisliğinde kullanılabileceği düşünülmektedir.

Anahtar Kelimeler: Klinoptilolit, Amfifilik kopolimer, Parçacık uzaklaştırma tekniği, Çözücüsüz kemik iskelesi üretimi, Toz sıkıştırma tekniği

To my country, my family and my lovely wife

ACKNOWLEDGEMENTS

The author wishes to express his deepest gratitude to his supervisor Assoc. Prof. Dr. Ayşen Tezcaner and cosupervisor Assoc. Prof. Dr. Dilek Keskin for their guidance, advice, criticism, encouragement and insight throughout the research.

The author also would like to thank Dr. Özge Erdemli for her help, suggestions and comments. In addition, the author would also thank Dr.Lütfiye Sevgi Özyeğin for her support and trust.

This study was supported by Middle East Technical University.
Project No: BAP-03-11-2014-001.

TABLE OF CONTENTS

LIST OF TABLES

TABLES

LIST OF FIGURES

FIGURES

LIST OF ABBREAVIATIONS

ALP: Alkaline Phosphatase

BCA: Bicinchoninic Acid

BSA: Bovine Serum Albumin

BTE: Bone Tissue Engineering

CaP: Calcium Phosphate

CL: caprolactone

CLN: Clinoptilolite

DMEM: Dulbecco's Modified Eagle Medium

DP_{PCL}: degree of polymerization of PCL

DP_{PEG}: degree of polymerization of PEG

DSC: Differential Scanning Calorimetry

ECM: Extracellular matrix

EG: Ethylene glycol

FBS: Fetal Bovine Serum

FT-IR: Fourier Transform Infrared Spectroscopy

HA: Hydroxyapatite

hFOB: Human fetal osteoblast

JCPDS: Joint Committee on Powder Diffractions Standards

M_n: Number average molecular weight

M_nPCEC: Number average molecular weight of PCEC

M_{nPCL}: number average molecular weight of PCL

M_{nPEG}: number average molecular weight of PEG

NaCl: Sodium chloride

$NaHCO_3$: Sodium bicarbonate

NMR: Nuclear Magnetic Resonance

PBS: Phosphate Buffered Saline

PCEC: PCL-PEG-PCL

PCL: Poly (ε-caprolactone)

PEG: Poly (ethylene glycol)

T_c: Crystallization temperature

T_d: Decomposition temperature

TGA: Thermogravimetric Analysis

T_m: Melting temperature

X_c: Percent crystallinity

XRD: X-Ray Diffraction

ΔH: Enthalpy of melting

ε-CL: ε-caprolactone

CHAPTER 1

INTRODUCTION

1.1. BONE

Bone is a hierarchical tissue that is constituted by several different types in humans: Long, short, flat, sesamoid and irregular bones (Figure 1). Although functionalities may vary, these bones possess outer compact bone layer, cortical bone, and internal spongy layer, trabecular bone (B.-S. Chang et al., 2000).

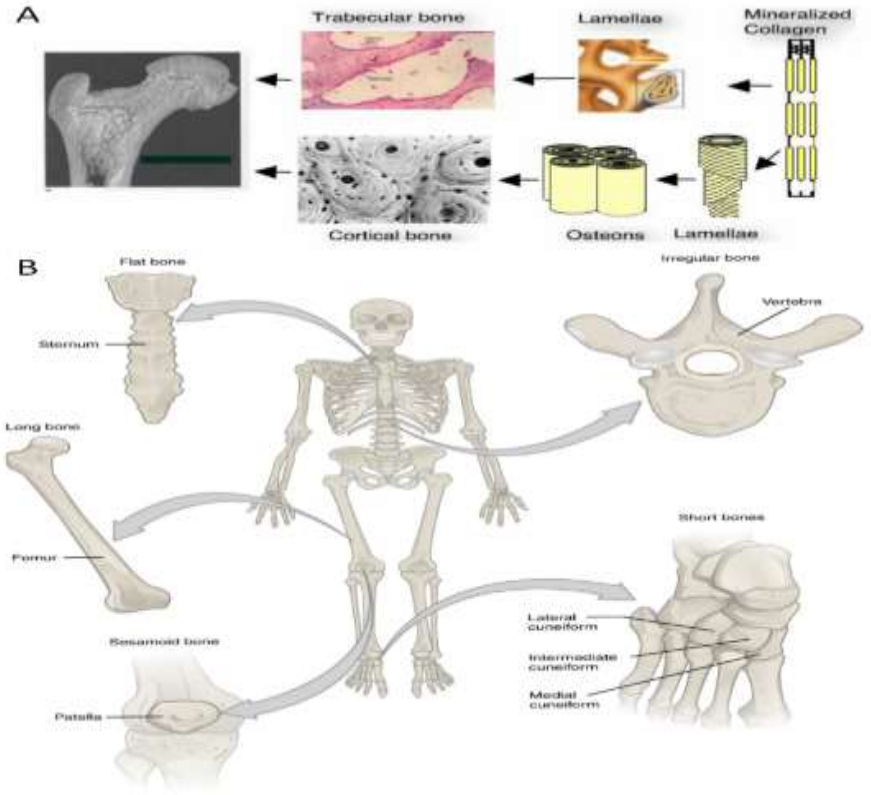

Figure 1. Hierarchical composition of bone tissue (A) and types of bones present in the human body (B) (X. Wang et al., 2010).

Bone tissue provides mechanical support for internal organs and tissues (Blanchard & Bronzino, 2012). Calcium, fat and sugar metabolism is partially controlled through bone-originated hormones (Clowes et al., 2005; Kindblom et al., 2009; Rosen, 2008). Furthermore, bone has a unique tissue formation which is called bone marrow (Reddi et al., 1977). Bone marrow is present in the spongy phase and solely responsible for accommodation and maintenance of hematopoietic and mesenchymal stem cell niche and osteoprogenitor cells (Morrison & Scadden, 2014), Figure 2). These cells are especially important to crucial steps of bone resorption and bone formation (Figure 2).

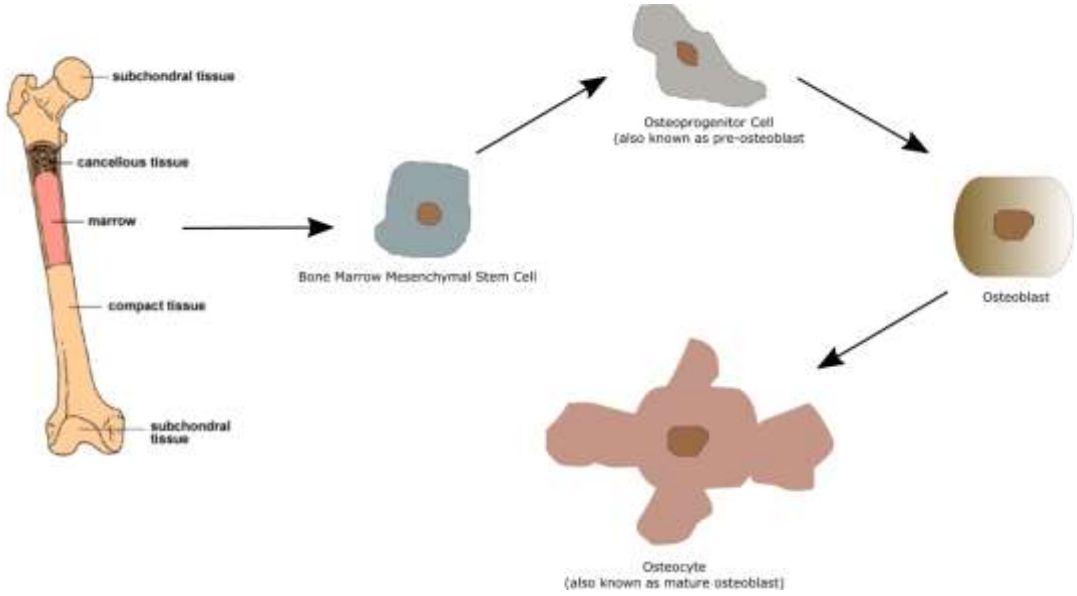

Figure 2. Mesenchymal stem cells (MSC) and hematopoietic stem cell (HSC) form the stem cell niche in bone marrow. MSC can differentiate stepwise into osteoprogenitor cell, then an osteoblast and finally into mature bone cell, osteocyte (Black arrows: Differentiation direction).

Osseous tissue (bone) is a biphasic composite tissue that is formed from organic and inorganic materials. The organic phase is in the form of complex natural polymers, which are proteins. Type I collagen is the major protein that forms the organic matrix and the rest of this phase is composed of non-collagenous proteins having diverse functions in the development and regeneration of bone. On the other hand, inorganic

phase contains mineral matrix which is in the form of stoichiometric hydroxyapatite ($Ca_{10}(PO_4)_6OH_2$, HA) (Glimcher, 1987) and water.

Type I collagen and non-collagenous proteins

Type I collagen is the most abundant protein in the organic phase of the bone (Rho et al.). It is secreted by osteoprogenitor cells and assumes a cross-linked triple helix structure. Moreover, type I collagen acts as a nucleation site for mineralization (Figure 4). Mineralized collagen fibers wrap around a central axis in compact stacks and eventually constitute the "lamellae" (Figure 3) (Webster & Ahn, 2007). Since the hierarchical structure of the bone shows that the lamellae bundles together to form "osteons", type I collagen can be deduced as the main substrate in the bone development (Henkel et al., 2013). Consequently, type I collagen influences the mechanical properties of the bone from microscopic level to macroscopic structure of the bone.

Non-collagenous proteins play important roles during osseous tissue maintaining, mineralization and remodeling. As described in the Table 1, non-collagenous proteins act as regulators of cellular attachment, differentiation and mineralization.

Table 1. Non-collagenous proteins in bone tissue.

Type of Non-collagenous Protein	Function	References
Osteopontin	Interaction with Ca^{2+} and regulation of bone remodeling	(Denhardt & Guo, 1993)
Osteocalcin	Facilitation of Ca^{2+} adsorption on collagen fibers	(Hauschka, 1986)
Bone Sialoprotein	Regulates bone formation and differentiation of osteoprogenitor cells to osteoclasts	(Malaval et al., 2008)
Alkaline Phosphatase – skeletal isoform	Regulation of mineralization by providing phosphate source in microenvironment	(Orimo, 2010)
Decorin	Modulation of collagen fiber formation and acting as an attachment site for bone morphogenic proteins	(von Marschall & Fisher, 2010)
Matrix GLA protein (vitamin K dependent gamma-carboxyglutamic protein)	Regulates bone formation by acting as an inhibitor of bone morphogenic proteins	(Wallin et al., 2010)
Osteonectin	Regulation of bone remodeling and repair, induction of osteoprogenitor cell differentiation to osteoblast and osteoclast	(Machado do Reis et al., 2008)

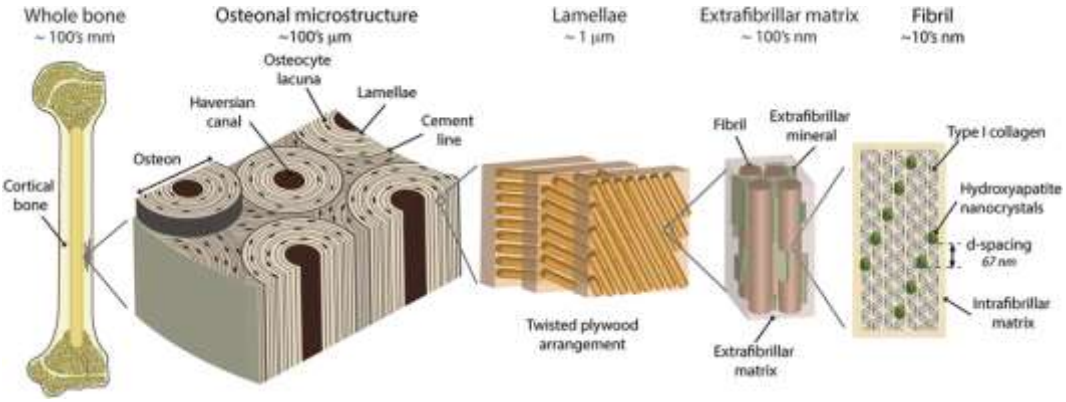

Figure 3. Hierarchical organization of bone structure. The formation of bone is initiated with mineralization of collagen fibrils (Webster & Ahn, 2007).

Hydroxyapatite (HA)

The inorganic phase of the bone is composed of a calcium phosphate mineral called apatite and its structure is generally termed as HA due to presence of hydroxyl ($-OH^-$) groups (Uskoković, 2015). In the core of the mineral crystal, Ca^{++} and PO_4^{-3} are present while OH^- units are in direct contact with the environment as shown in Figure 4 (Wopenka & Pasteris, 2005).

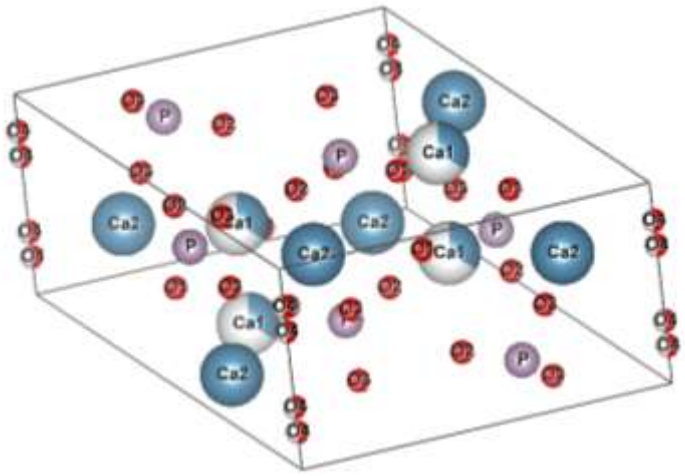

Figure 4. Crystal structure of HA.

As the mineral and collagen matrix are wetted by the water (7% (w/w) of total bone tissue), Ca^{++} ions of the mineral phase can trigger coordination between HA and

collagen molecules (Dorozhkin, 2015). Ca^{++} ions present in apatite interacts through carboxylate of the collagen molecules (Rhee et al., 2000). Therefore, mineral phase of bone can coat the lamella during bone growth (Clarke, 2008). Layer by layer, from lamella to osteons, HA deposition confers uniaxial compressive strength to the bone tissue (Figure 3).

1.2. BONE DEFECTS

Bone structure is comprised of both organic and inorganic phases as explained previously. In order to maintain tissue integrity during development and regeneration, these phases are in dynamic contact through multiple pathways. Osteogenic cells are exposed to biological and mechanical signals daily and they trigger the bone specific phenomenon known as “bone remodeling” (Figure 6)(Hadjidakis & Androulakis, 2006).

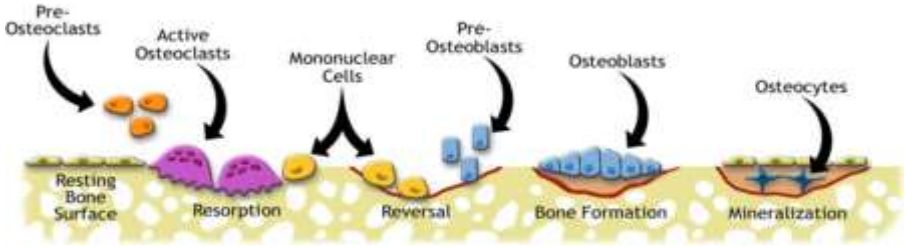

Figure 5. Bone remodeling process involves various types of cells which function collectively to restore bone structure

Remodeling defines the production of new bone tissue on the existing bone layer while preexisting layer is resorbed (Hollinger et al., 2004). Daily routine of remodeling process is initiated by microdamages (internal microcracks) which do not trigger whole tissue repair (Figure 6A).

Figure 6. The general overview of bone defects. Microcracked bone structure (A), bone underwent tumor resection operation (B), critical size damage or segmentally fractured bone (C) and bone having congenital defect such as scoliosis (D).

The concept behind remodeling was first postulated by Wolff to explain the primary observations on physiological changes of bone during exhausting mechanical stimuli and absence of mechanical stimuli (Mazhuga, 1984). As the concept of dynamic response of bone develop, scientist uncovered the main aspect of remodeling process: Cell to cell interactions and how bone cells react to environmental conditions where they fire and divert bone specific responses and ultimately undergo remodeling (Hench & Polak, 2002). The cells responsible for bone resorption, remodeling and maintenance are given in Table 2.

Table 2. Cells present in bone tissue.

Cell	Function	Reference
Pre-osteoblast	Osteoprogenitor cells which differentiates into mature osteoblasts	(Shea et al., 2000)
Osteoblast	Bone forming cells that are responsible for bone tissue growth and mineral deposition	(Capulli et al., 2014)
Osteoclast	Bone resorbing cells which help to reshape and reform the bone microenvironment	(Florencio-Silva et al., 2015)
Osteocyte	Entrapped osteoblasts within mineral phase of bone during deposition. Function during bone development, responsible for cellular activities of bone tissue.	(Dallas et al., 2013)

Although bone tissue has innate ability of self-regeneration the tissue upon injury, defects that are critical in cannot be repaired spontaneously (Y. Li et al., 2015).

Bone structure trauma and defects can create substantial damage on the tissue. These injuries can be classified under congenital defects which result in progressive damage on bone tissue, bone loss due to tumor resections, infections such as osteomyelitis, fractures leading to partial fragmentation and critical sized defects formation due to segmental defects (Figure 6).

1.3. CONVENTIONAL TREATMENTS

Recent developments in surgical procedures and understanding of the physiology behind bone defects led to improvement in bone trauma and defect treatments (Geris et al., 2009). Over the many procedures, the critical sized defects are currently been mended by Masquelet technique (Lasanianos et al., 2010) that provides internal operation through pseudomembranes from autograft, Ilizarov technique (Keating et al., 2005) containing external fixation with the use of circular frames or plates, and direct autografting which is pronounced as a gold standard (Gómez-

Barrena et al., 2015). However, all of the standardized procedures for bone reconstruction and repair fall short because of problems associated with the requirement of multiple operations, limited donors, donor morbidity during and after the procedure, whole body immunosuppression for very long time period and possible disease transmission (Oryan et al., 2014). As a result, traditional bone repair operations and techniques have various disadvantages and limited choices to overcome. For this purpose, bone tissue engineering was developed and conjoined into the literature (Dimitriou et al., 2011).

1.4. BONE TISSUE ENGINEERING

Bone tissue engineering (BTE) aims to restore the loss of function and ensure de novo bone tissue formation in order to overcome present disadvantages of current therapies (Black et al., 2015). In order to ensure bone tissue regeneration, scaffolds which are also known as "tissue engineering constructs" have been produced and studied (Woodruff et al. 2012). Scaffolds are primarily designed to improve cell viability, proliferation, osteogenic differentiation as well as providing a temporary mechanical support for the replenishing bone tissue (Henkel et al., 2013). Consequently, BTE offers an alternative approach to the traditional treatments using preferably biomimetic scaffolds (Bose et al., 2012). These scaffolds are expected to be biocompatible and biodegradable (Puppi et al., 2010; J. Wang & Yu, 2010). In addition, osteoinductivity and osteoconductivity are important parameters for any BTE scaffold (Corrales et al., 2014). Osteoconductivity refers to bone growth on a surface while osteoinduction attributes to induction of the primitive cells (stem cells) to differentiate into bone phenotype (Daculsi et al., 2013). Specifically, osteoconduction follows osteoinduction in practical sense. Development of mature bone cells from osteoprogenitor cells both enable colonization of the scaffold in defect environment and provide a substrate for cells to deposit bone mineral leading to fusion of bone to scaffold and subsequent growth of bone through the scaffold (Albrektsson & Johansson, 2001).

In order to meet the criteria explained above and thus to produce successful BTE scaffolds, natural and synthetic polymers, ceramics, and their composites are the materials used in scaffold fabrication.

1.4.1. Types of Materials

1.4.1.1. Polymers

In BTE applications, polymeric materials draw much attention due to having several very important properties. These materials can offer immense versatility such as biodegradability, biocompatibility, tailor-made shape, size, degradation rate matching bone tissue regeneration rate, high surface to volume ratio for adsorption of bone related biological molecules etc. (Makadia & Siegel, 2011).

Polymeric materials can be obtained from natural sources or designed synthetically. Although natural polymers are biocompatible, they still cause problematic conditions in in vivo systems. Owing to be produced from a natural source, xenogeneic or allogeneic biological molecules lead to extensive inflammatory response and disease transmission (Badylak & Gilbert, 2008). Moreover, natural polymers lack desired processability and are highly expansive even in small quantities (Sabir et al., 2009). On the other hand, synthetic polymers can be designed on demand to be biodegradable and biocompatible without any inflammatory response (Nair & Laurencin, 2007). Furthermore, the polymerization reactions can be monitored and controlled. As a result, intrinsic properties of the fabricated molecules can be altered and thus their processability is very high. Therefore, hydrophilicity or hydrophobicity, size of the polymer chains, functional groups on the chains, additional introduction of biological molecules to the synthetic polymers can be managed easily (Kohane & Langer, 2008).

Biocompatible synthetic polymers such as poly(ε-caprolactone) (PCL) and poly(ethylene glycol) (PEG) have been frequently used in the studies related to BTE as scaffold materials because of their biocompatibility, non-cytotoxic degradation products, easily tailored degradation rates and porosity (Bose et al., 2012; Kutikov & Song, 2013; Lin et al., 2013; Yang & Pierstorff, 2012).

1.4.1.2. Poly (ε-caprolactone)

Poly e-caprolactone (PCL) is an aliphatic polyester that can be synthesized from the monomer e-caprolactone (Figure 7). PCL appears as one of the most commonly used synthetic polymers in BTE scaffolds due to its biocompatibility and FDA-approved non-cytotoxicity (K. Y. Chang et al., 2009; Erdemli et al., 2010). PCL has a high degree of crystallinity and hydrophobicity, thus it has long degradation time, nearly 3 or 4 years in vivo (Woodruff and Hutmacher, 2010). Slow in vivo degradation kinetics of pure PCL scaffolds may also restrict their usage as a versatile matrix material and native bone tissue regeneration can be inefficient within pure PCL scaffolds. In order to address this inconveniency, PCL blends with hydrophilic and quickly degrading functional polymers or PCL composite scaffolds with bioactive molecules have been widely used in BTE. For example, PCL can be utilized in composite scaffold production with natural polymers such as gelatin, alginate and collagen to improve cellular attachment, wettability and biodegradation rate of PCL (Chong et al., 2007; Gautam et al., 2013; Y. B. Kim & Kim, 2015). Preparation of composite scaffolds including inorganic bioactive ceramics such as HA with PCL has also been studied in the literature and these scaffolds displayed enhanced bioactivity and hydrophilicity (Heo et al., 2009; J. Zhao et al., 2008).

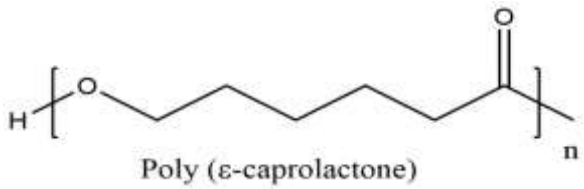

Figure 7. Chemical structure of PCL.

1.4.1.2. Poly (ethylene glycol)

Poly (ethylene glycol) (PEG) is a biocompatible polymer that can be readily hydrolyzed because of its high hydrophilicity (Figure 8). In addition, PEG has been approved by the U.S. FDA for internal use in biomedical research and applications (Knop et al., 2010). Although unmodified PEG is a non-biodegradable polymer, smaller PEG units than 30 to 50 kDa size can be readily removed from kidneys and

can be utilized efficiently in synthetic composite polymer production without compromising biocompatibility (Veronese & Pasut, 2005).

In recent years, PEG has been used in bone tissue constructs for increasing hydrophilicity and degradability of scaffolds by incorporating with other polymers and bioactive molecules (Niu et al., 2014; Serra et al., 2014). PEG can be notably utilized in bone tissue applications safely to improve cellular attachment, cellular guidance and biocompatibility (C. Dahlin et al., 2014; Kinard et al., 2013).

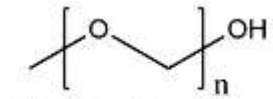

Poly (ethylene glycol)

Figure 8. Chemical structure of PEG.

1.4.1.3. Poly (ε-caprolactone)-poly (ethylene glycol)- poly (ε-caprolactone)

PEG has been used to form various block copolymers with PCL (Fan et al., 2013; Sosnik & Cohn, 2003). PEG-PCL copolymers are biodegradable and biocompatible and they have been widely investigated for use in BTE as scaffold material (Fu et al., 2013; Hoque et al., 2009). The most extensively used method for synthesis PEG-PCL copolymers is ring-opening polymerization from ε-CL and PEG with catalyst (C. B. Liu et al., 2008). By using this polymerization method, ratio of PCL/PEG can be modulated to fabricate distinct copolymers with varying thermoplasticity, degradability and hydrophilicity (M. H. Huang et al., 2004). In this regard, PCL-PEG-PCL (PCEC) scaffolds were studied not only for their biocompatibility and biodegradability but also for their ability to form blends, composites and to incorporate bioactive molecules without damaging their structures (Figure 9) (Moon et al., 2002). However, scaffolds produced from a pure synthetic polymer may lack bioactivity thus may not show osteoconductive or osteoinductive properties. In order to overcome this situation, synthetic polymers are generally combined or blended with other material types such as ceramics to enhance their use as BTE scaffold materials.

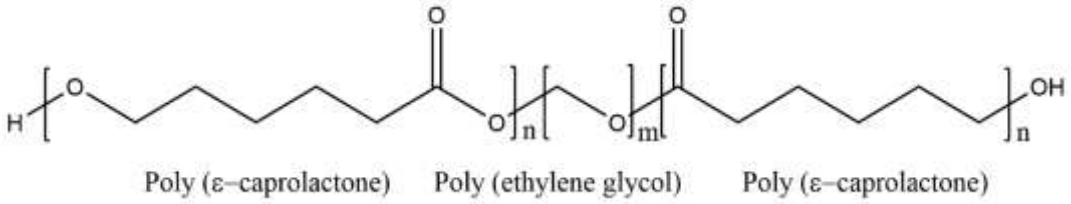

Figure 9. Chemical structure of PCEC.

1.4.1.2. Ceramics

In BTE applications, ceramics are highly utilized due to similarities between inorganic phase of the bone tissue and ceramics. One of the most widely studied bioactive ceramic class is calcium phosphate bioceramics (CaP). CaP is a bioactive, osteoconductive, osteoinductive and biocompatible ceramic which is used in BTE constructs such as scaffolds. The bioactivity of CaP originates from the ability of releasing ions that dynamically influences the biological environment both in vitro and in vivo (Poologasundarampillai et al., 2014). The release of osteogenic ions such as Ca^{++} triggers the nucleation of HA, improves cellular attachment through focal adhesions and also osteogenic differentiation. However, the solubility of the ceramics in biological environment brings in a limitation for their biodegradability and osteoinductivity (Sainz et al., 2010). In the form of HA, the brittleness of the material increases as well as biodegradability and osteoinductivity declines. On the other hand, CaP solubility and biodegradation accelerate as the CaP is synthetically transformed into amorphous nature such as amorphous calcium phosphate (Barrère et al., 2006). Consequently, mechanical strength of CaP decreases and degradation kinetics outmatches the natural bone formation thus preventing its use as a successful bioceramic in BTE (LeGeros et al., 2003; Jie Zhao et al., 2011). Therefore, CaP bioceramics are generally doped with several osteoinductive ions such Si, Mg, Sr, Zr etc. or sintered with other bioactive materials such as silicate (SiO_4) to yield osteoinductive CaP (Demirkiran et al., 2010; H. Li & Chang, 2013; Maier et al., 2004; Pietak et al., 2007; Saidak & Marie, 2012) to improve bioactivity and cellular interaction.

In literature, ceramic materials obtained from natural sources were also studied, characterized and employed in bone tissue scaffolds. As an advantage over synthetically produced ceramics, these materials can be obtained in vast amounts. Naturally formed ceramics generally possess silicate backbone that may enhance bone specific cells to proliferate and differentiate. As example, montmorillonite and hallosite were used as inorganic component of a composite bone tissue scaffold to improve cellular adhesion, bioactivity and mechanical properties of polymer based bone scaffolds (Aneta J. Mieszawska et al., 2011; Naumenko et al., 2016). In addition, zeolites were employed as a corrosive resistant biocompatible coating on $Ti_{10}Al_4V_6$ implants for bone tissue and as an inorganic filler used in gelatin/zeolite scaffold and as anti-hypoxic agent for fibroblasts (Bedi et al., 2009; Ninan et al., 2013; Seifu et al., 2011)

1.4.1.2.1. Zeolites

Zeolites have backbones formed by SiO_4 and Al_2O_3 groups attached together by oxygen atoms forming crystalline aluminosilicate ceramic (Figure 10).

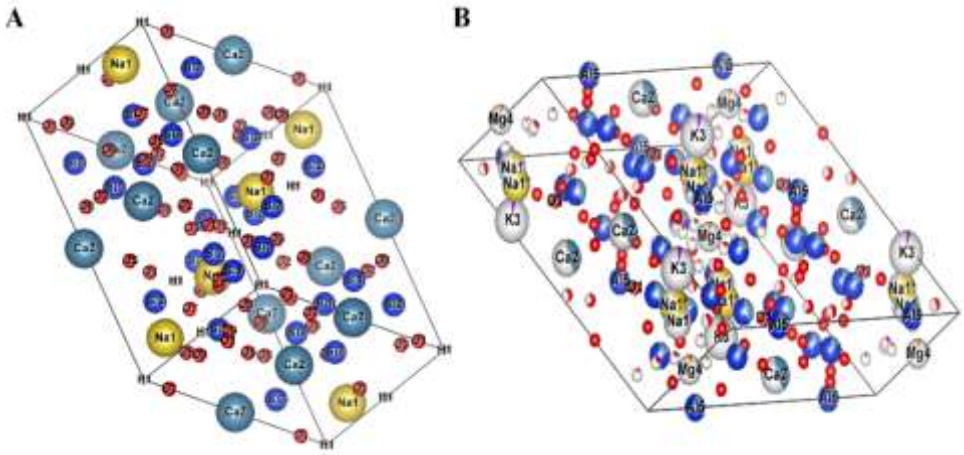

Figure 10. Crystal structures of zeolite (A) and clinoptilolite (B).

In general, zeolites show bioactivity and biocompatibility (Fatouros et al., 2011). By increasing alkaline phosphatase and osteocalcin synthesis, zeolites boost proliferation and differentiation of osteoblasts (Schainberg et al., 2005; Yu et al., 2013). The ability of biomolecule adsorption on the surface of the zeolites makes them

potential carriers for various biological agents such as albumin, thrombin and cyclodextrin (Akgül, 2008; Yunlong Li et al., 2014; Szarpak-Jankowska et al., 2013).

Clinoptilolite (CLN) is a biocompatible natural zeolite made of aluminosilicate (Al_2SiO_5) backbone ionically bound to osteogenic ions such as Mg^{2+} and Ca^{2+} as seen in Figure 10B and possess various Si/Al ratios which leads to various levels of hydrophilicity (Cundy & Cox, 2003; Uyumaz et al., 2011). In addition, the ionic nature of clinoptilolite provides an opportunity for protein adsorption. In a previous study, neutral, acid and base treated clinoptilolite samples with different Si/Al ratio showed a very high adsorption capacity for bovine serum albumin (BSA) and a significant increase in the amount of adsorbed BSA was observed at the acid and base treated clinoptilolite samples compared to natural ones (Akgül, 2008). In addition, clinoptilolite showed improvement in bioactivity of osteoblasts and enhanced new bone formation (Schainberg et al., 2005). As a result, it is thought that blending polymers with clinoptilolite may enhance osteogenic characteristics of the BTE scaffolds.

1.4.1.3. Composites

A composite material is termed as a specific combination of various materials into a different composition or structure to obtain best properties of the combined materials (Gloria et al., 2010; Nicolais et al., 2010). Composite materials provide an opportunity to fabricate a new material that shows synergistic properties of the individual materials (Callister & William D., 2007). For this purpose, various material couples such as bioceramics and synthetic polymers are combined together to overcome the respective limitations during the production of BTE scaffolds.

The optimal design of a BTE scaffold includes osteoconductive, osteoinductive properties as well as physical properties such as a three-dimensional, interconnective, porous and mechanically strong template which can be biodegraded as the bone tissue regenerates (Moroni et al., 2008). The combination of synthetic polymers and bioceramics opens up a new area of design not only for improved degradation and ion release characteristics for bioceramics but also for strong overall mechanical

properties of a porous scaffold (Rezwan et al., 2006). The resultant effect of the combination of these materials can be exploited to obtain a successful BTE scaffold.

In this study, PCEC was used as a synthetically produced copolymer to act as a matrix while CLN functions as a bioactive ceramic material that is dispersed within the polymeric matrix. This combination will serve as an efficient BTE scaffold that can be in various shapes, sizes and porosities. The individual limitations of these materials and the expected properties of final product of their composite is given in the Table 3.

Table 3. The properties of PCEC, CLN and their composite.

Material	Advantages	Disadvantages
Synthetic Polymer (such as PCEC)	Biocompatibility and bioresorbability Retention of mechanical strength for long time	Lacking bioactivity
Bioactive ceramic (such as CLN)	Bioactivity due to presence of osteogenic ions such as Mg2+, Ca2+, SiO2 Biodegradation of ceramic material	Lacking osteoinductivity and biodegradability Brittle structure
Composite (such as bioactive ceramic and polymer)	Osteoconductivity and osteoinductivity Tailorable degradation, size, porosity and mechanical strength	

1.4.2. Scaffold Guided Techniques

BTE scaffold fabrication should produce a final structure that must provide following properties:

- Scaffold Integrity: The integrity of the scaffold should persist throughout the period of bone regeneration because cellular attachment, proliferation and subsequent production extracellular matrix occurs on a mechanically strong substrate (Logeart-Avramoglou et al., 2005).
- Scaffold Porosity: Osteoconduction is directly related with the overall porosity of the scaffold that enables bone ingrowth. The bone ingrowth phenomenon occurs into the pores while cells invading the scaffold can exchange nutrients, gases, biological factors etc. (Smith et al., 2010).
- Biomimicking: Besides being a mechanically strong substrate, a scaffold should also function to enhance biological factor availability in the microenvironment of the bone defect (Amini et al., 2012) As a result of biomimicking environment, cells function to repair bone defect faster without adverse effects such as scar tissue formation and immunological response due to unmatched density and surface characteristics which may lead to scaffold failure (Fong et al., 2011). Ability of the scaffold to adsorb proteins such as collagen in defect microenvironment and successfully presenting them to cells can induce osteoprogenitor cells to proliferate, differentiate and eventually mature into bone phenotype (Harvey et al., 2010).

To combine diverse properties required for cellular growth, colonization, differentiation into bone-specific lineage while providing a mechanically stable environment, 3D BTE scaffolds are produced through various methods. In each of these methods, there are several advantages and disadvantages associated with materials used, reproducibility of the technique and the properties of final scaffold.

1.4.2.1. Electrospinning

Electrospinning method utilizes voltage difference between the feeding solution of polymer, polymer blends or polymer-ceramic blends and the collector (Bhardwaj & Kundu, 2010). Small diameter filaments at micrometer or nanometer scale are produced through electrospinning method to improve cellular adhesion as well as biological molecule adsorption to final structure due to increased surface area to volume ratio. However, the structure produced through conventional electrospinning process lacks pore sizes enough to support cellular invasion and appears as if a 2D

fiber mesh rather than a 3D network or a scaffold (Dalton et al., 2013). In addition, electrostatic repulsion during the process inhibits direct control over the procedure and handling the resultant structure is very difficult (Centola et al., 2010). On the other hand, the alternative approach of this method is wet electrospinning. In this method, the non-solvent system of the used polymer blend acts as the collector system enabling the production of 3D scaffold with larger diameter of fibers (Atila et al., 2015). As explained in the literature, higher diameter values for electrospun fibers may improve pore sizes of the structures (R. L. Dahlin et al., 2011). However, both methods suffer from weak mechanical strength thus electrospinning method is highly recommended for soft tissue engineering rather than production of BTE scaffolds (Zhu et al., 2015).

1.4.2.2. Melt Spinning

In order to overcome several drawbacks met in the electrospinning method such as requirement of organic solvents that can both dissolve the polymer and carry electrical charge, melt spinning method was developed (Dalton et al., 2007). The melt spinning method can result in fiber stacking so that 3D network structures may be obtained. In addition, pore sizes may be up to orders of hundreds of microns to enhance cellular invasion (Karageorgiou & Kaplan, 2005). The stacking of deposited fibers during the procedure also mechanically strengthens the final structure and provides better handling (Brown et al., 2011). Although the method is straightforward, there are fundamental requirements to be met in order to apply melt spinning protocol. The polymeric materials used in this method should be thermosetting polymers and as a result, the final products are generally brittle (Zaiss et al., 2016). Moreover, the main limiting factor is the polymer viscosity. Consequently, application of melt spinning method to polymer blends and polymer-ceramic blends leads to unexpected final products and diminishes control over the procedure due to drastic changes in viscosity during blending (Cui et al., 2015).

1.4.2.3. Solvent Casting

Solvent casting, also known as porogen leaching method, is a traditional method in which polymer solution in organic solvent is mixed with a bioactive ceramic and porogen (Thadavirul et al., 2014). The dissolution of polymer is blended thoroughly

with the other components to disperse them effectively. The mix is then added into a mold where it is either freeze-dried or air-dried to remove organic solvent (Taqvi & Roy, 2006). After that, the dried mix is introduced with another solvent that dissolves the porogen while polymer matrix and the ceramic material in the polymer matrix stay intact. Using this method, mechanically strong and scaled up production can be obtained while pre-determined shape of the final structure may be controlled. On the other hand, the main disadvantage of this protocol is the use of organic solvent that cannot be removed completely in the final structure thus leading to non-biocompatibility (Stevens et al., 2008). Moreover, reproducibility, pore homogeneity and pore interconnectivity could be very low (Leong et al., 2003). Since the ceramic materials possess higher density than the polymer matrix, they may settle down during the procedure and homogeneity of the final structure could be compromised (Liao et al., 2002).

1.4.2.4. Melt Molding

To overcome the limitations of solvent casting method, melt molding method is usually employed. The molds having desired shape and size are filled with the polymer blends or polymer-ceramic blends and heated over the glass transition temperature of the polymer used (Thomson et al., 1995). For acquiring a porous scaffold, the melt blend is also mixed with an appropriate porogen (Haugen et al., 2004). The mix is either compressed or air-dried within the mold. The limitations observed with melt molding method are several: Limited choice of polymers to work with, high temperature requirements and high possibility of heterogeneous mix of polymer-ceramic-porogen reduce the reproducibility of this method (Leong et al., 2003; Scaffaro et al., 2016).

1.4.2.5. Compression Molding

Compression molding is another traditional method and widely used in which component of the BTE scaffolds are dry mixed and compressed (Mathieu et al., 2006). The parameters effecting the final product are the pressure employed to compress the scaffolds and the level of component homogeneity during mixing. Consequently, the major advantage of this technique is the predictability of porosity, pore size and shape

of the final product (G. X. Huang et al., 2015). In addition, avoidance of organic solvent usage during preparation of the scaffold is another important factor for tissue engineers to utilize this method.

Compression molding method is a highly compatible method that can be combined with any other scaffold preparation method aforementioned (Kane et al., 2015). As stated in Siddiq et al., compression molding can be easily combined with porogen leaching method without the use of any organic solvent (Siddiq & Kennedy, 2015). Furthermore, the amount of porogen, pressure for compression and time of compression can be controlled very efficiently to produce BTE scaffolds successfully. Although the final product is mechanically strong and highly porous, reproducibility is a major concern (Lo Re et al., 2015). The reason for lack of reproducibility is basically the inability to mix the components homogenously. Because size and density of the individual particles play important role in mixing of scaffold components. For this reason, dispersion of the components in a solution which is a non-solvent for all components may help to overcome homogeneity problems.

1.4.2.6. Solvent Free Powder Compression / Salt Leaching Technique

Current methods for fabrication of BTE scaffolds have various drawbacks as aforementioned. Limited choice of polymer, inability to blend different types of materials, application of organic solvent to improve homogeneity of polymer-ceramic-porogen blend and obtaining a mechanically strong scaffold with high porosity and interconnectivity are major challenges to overcome during the production of a successful BTE scaffold. In addition, recent studies in the field of BTE scaffold production involve various methods employed at the same time. Combination of the aforementioned methods led to development of 3D BTE scaffolds overcoming limitations of the methods used in the process. As proposed by Gürbüz et al., multi-layer membrane production through solvent casting/particulate leaching technique in combination with electrospinning may provide a 3D scaffold structure supporting cellular ingrowth as well as bioactive molecule transport (Gürbüz et al., 2016). Although this method provided a 3D scaffold, which may act as a successful ECM constructs, it still lacked mechanical strength. In addition, one of the widely used

methods for successful BTE scaffold preparation is compression molding method. As an example, Zhang et al. employed high pressure compression molding/particulate leaching combined technique with solvent casting to provide a homogeneous blending of the components and then fusion of polymer particles under high pressure compression (Zhang et al., 2016). However, this method still lacked the efficiency to employ reproducibly because of inability to blend individual scaffold components successfully since organic solvent use with bioceramic materials leads to agglomeration of bioceramic particles and overall heterogeneous blending between bioceramic and polymer matrix owing to electrostatic repulsion (Kothapalli et al., 2008; Liang et al., 2011; Müller et al., 2014).

In order to overcome problems aforementioned for the production of 3D BTE scaffolds, several precautions can be taken:

- The components of the scaffolds such as polymer, ceramic and porogen can be mixed in a liquid environment whose liquid phase can be removed easily at the end of the procedure and does not act like an organic solvent for polymer.
- If compression molding method is employed, relaxation supports can be used as a part of mold in order to prevent over-compression and provide relaxation of polymer by energy dissipation (Azhdar et al., 2005).
- Polymer phase can be downsized, i.e. polymer aggregations can be crushed into powder form without damaging chemical and physical properties of the polymer such as chain length.

1.5. AIM OF THE STUDY

Tissues may undergo critical-sized defects which cannot be repaired through native processes. In order to initiate regeneration, tissue-specific engineered constructs can be applied. Recent advances in the field of BTE mainly focus on the development of engineered constructs such as BTE scaffolds in which patient-specific cells proliferate and differentiate into mature bone cells for regenerating new tissue.

BTE scaffolds can be prepared by various methods. However, tissue engineers still lack properly designed, reproducible and straightforward scaffold preparation methods. In order to overcome this problem, solvent free powder compression / salt leaching technique was employed. With this method, it was aimed that scaffold components could be blended homogenously and reproducibly compressed into mechanically strong, interconnective, porous, osteoinductive and osteoconductive BTE scaffolds. For improving osteoinductivity and osteoconductivity, we hypothesized that composite PCEC-based scaffolds might be prepared with a natural zeolite, CLN, that could provide protein adsorption and encourage new bone formation while increasing mechanical strength and bioactivity of the copolymer-based scaffolds. Therefore, novel CLN/PCEC BTE scaffolds may act as promising 3D cell carriers for enhancement of bone regeneration in BTE applications.

PCEC triblock copolymer was synthesized by ring-opening polymerization and triblock copolymer was characterized by differential scanning calorimetry (DSC), thermogravimetric analysis (TGA), proton nuclear magnetic resonance (^{1}H NMR) spectroscopy and Fourier transform infrared (FT-IR) spectroscopy. The effect of CLN content on scaffold properties such as morphology, porosity, mechanical, in *vitro* bioactivity, degradation and water uptake properties was investigated. Protein adsorption capability of scaffolds was also examined by incubating CLN/PCEC composite and pure PCEC scaffolds in fetal bovine serum (FBS) solution. Additionally, proliferation, and osteoblastic differentiation of the human fetal osteoblast cells (hFOB) on the scaffolds were evaluated with *in vitro* cell culture studies. It is the first time CLN/PCEC scaffolds were prepared and analyzed for BTE applications. Furthermore, the CLN/PCEC scaffolds were produced with different porogen sizes to determine the feasibility of the method.

CHAPTER 2

MATERIALS AND METHODS

2.1. MATERIALS

Deoxyribonucleic acid from Calf thymus, PEG (M_n: 4000 kDa), ε-caprolactone (pure, 97%), sodium bicarbonate ($NaHCO_3$), calcium chloride dehydrate ($CaCl_2.2H_2O$), o-cresophtalein, 8-hydroxyquinone-5-sulfonic acid and 2-amino-2-methyl 1,3-propanediol were purchased from Sigma-Aldrich (MO, USA). Dibutyltin dilaurate, sodium chloride (NaCl) and methylene blue dye were obtained from Merck (NJ, USA). Sodium dodecyl sulfate was purchased from Biorad (CA, USA), Prestoblue, Alamar Blue, Hoechst 33258 from Invitrogen (MA, USA), Alkaline Phosphatase Analysis kit and Osteopontin Analysis kit from Abcam (Cambridge, UK) and . All other chemicals used in the study were of reagent grade and used as purchased.

2.2. METHODS

2.2.1. Synthesis and Characterization of PCEC

PCEC triblock copolymer was synthesized by ring opening polymerization of ε-caprolactone (ε-CL) initiated by PEG in the presence of dibutyltin dilaurate as a catalyst (Sosnik & Cohn, 2003). Briefly, PEG was introduced into a 3-neck flask in liquid vaseline bath and kept in 100°C for 30 min under N_2 atmosphere to remove moisture. Then, ε-CL with (PEG/ε-CL 1:24 (w/w)) feed ratio and dibutyltin dilaurate with a concentration of 0.5% of total reactants were added and the mixture was stirred at 140°C for 24 h under N_2 atmosphere. After cooling to room temperature, the resultant triblock copolymer was dissolved in dichloromethane and precipitated by adding excess amount of ethanol to remove the catalyst and residual ε-CL. The precipitate was then filtered, washed with ethanol several times and dried at 40°C in vacuum oven for 3 days.

The chemical compositions of PEG and PCL homopolymers and PCEC triblock copolymer were studied with Fourier transform infrared (FT-IR) spectroscopy (Bruker IFS 66/S, FRA 106/S, Karlsruhe, Germany) and proton nuclear magnetic resonance (^{1}H NMR) spectroscopy (Bruker Biospin, Rheinstetten, Germany). The number average molecular weight (M_n) of copolymer was determined by ^{1}H NMR analysis. The calculation of M_n value, degree of polymerization and PCL/PEG ratio of synthesized triblock copolymer was based on the integrity ratio of the ^{1}H NMR peaks at 4.07 ppm belonging to methylene protons (-CH_2-) of PCL segment and 3.65 ppm (-CH_2-) belonging to PEG segments. Equations 1, 2 and 3 were used in the calculations as given below (M.-H. Huang et al., 2003):

$$\overline{DP}_{PEG} = \frac{M_{n^{PEG}}}{44} \quad (1)$$

$$\overline{DP}_{PCL} = \frac{M_{n^{PEG}}}{44} x \frac{[CL]}{[EG]} \quad (2)$$

$$M_n = M_{n^{PEG}} + 114x\overline{DP}_{PCL} \quad (3)$$

where 44 (g/mol) and 114 (g/mol) correspond to the molecular weights of ethylene glycol (EG) and linearized caprolactone (CL), respectively (M. H. Huang et al., 2004). DP shows the degree of polymerization for each of the homopolymer and it was used to detect the number average molecular weight of PCEC (M_{nPCEC}).

Additionally, the thermal properties of PCL, PEG homopolymers and PCEC copolymer were determined by using thermogravimetric analysis (TGA, Perkin Elmer, Waltham, MA, USA) and differential scanning calorimetry (DSC, Perkin Elmer, Waltham, Massachusetts, USA). Decomposition temperature (T_d) was determined by TGA and melting temperature (T_m), crystallization temperature (T_c), enthalpy of melting (ΔH) and percentage of crystallinity (X_c) of PEG, PCL homopolymers and PCEC triblock copolymer were determined by DSC. X_c of the homopolymers and PCEC triblock copolymer were calculated using the M_n values of PCL, PEG homopolymers and PCEC copolymer obtained from ^{1}H NMR spectra as given in the Equations 4, 5 and 6:

$$Xc_{\ PCL}(\%) = \frac{\Delta H_m{}^{1}{}_{PCEC}}{\Delta H_m{}^{2}{}_{PCL}} x100 \quad (4)$$

$$Xc_{PEG}(\%) = \frac{\Delta H_m{}^1{}_{PCEC}}{\Delta H_m{}^2{}_{PEG}} x100 \quad (5)$$

$$Xc_{PCEC}(\%) = X_{c_{PCL}} x \frac{M_{n_{PCL}}}{M_{n_{PCEC}}} x100\% + X_{c_{PEG}} x \frac{M_{n_{PEG}}}{M_{n_{PCEC}}} x100\% \quad (6)$$

where $\Delta H_m{}^1$ represents experimental enthalpy of melting of PCEC while $\Delta H_m{}^2$ shows theoretical enthalpy of melting of 100% crystalline PCL and PEG homopolymers. M_{nPCL}, M_{nPEG} and M_{nPCEC} represent M_n values evaluated from the integrity ratio of the ^{1}H NMR peaks for each homopolymer and triblock copolymer.

2.2.2. Characterization of CLN

2.2.2.1. Surface Morphology, Chemical and Structural Composition of CLN

Surface morphology and chemical composition of CLN were determined by using electron scanning electron microscopy (SEM, JSM-6400, JEOL, Tokyo, Japan) and energy-dispersive X-Ray spectroscopy (EDS) analysis equipped with SEM, respectively. Moreover, structure of the CLN was analyzed through X-Ray Diffraction technique (XRD, D8 Advance, Bruker, Germany) employing CuKα radiation at 40 kV/30 mA to confirm the structure of CLN with the standard (JCPDS No: 025-1349).

2.2.2.2. Particle Size and Zeta Potential of CLN

The mean particle size and particle size distribution of CLN were determined via wet dispersion in deionized water (dH_2O) without the use of any surfactants (DLS, Malvern CGS-3, Langen, Germany). Particle size dispersity (SPAN) was calculated by Equation 7 where d[0.9], d[0.5] and d[0.1] represent 90th, 50th and 10th percentiles respectively (Erdemli et al., 2015):

$$SPAN = (d[0.9] - d[0.1])/d[0.5] \quad (7)$$

Previous to fabrication of scaffolds, CLN was filtered through 50 μm mesh, degassed under vacuum at 100°C. Electrostatic stability of CLN at various pH values was determined with zeta potential (ζ) analysis within pH range from 2 to 11 (Malvern Nano ZS90, UK).

2.2.2.3. Protein Adsorption on CLN

Classical batch equilibration method was employed to measure the protein adsorption capacity of the CLN quantitatively. Fifty mg of CLN was added to 10 ml

BSA solution (10 mg BSA in 10 ml of 0.1 M phosphate buffered saline, PBS) of various ionic strengths (0.05, 0.1 and 0.15 M NaCl in water) and magnetically stirred. After that, the solution was centrifuged at 15000 rpm to collect the supernatant containing non-adsorbed BSA. Protein content in the supernatant was measured by using micro bicinchoninic acid (μBCA) assay. Supernatant was added in BCA working solution containing 50 parts of BCA and 1 part copper sulfate pentahydrate (4%) and then the optical density at 562 nm was measured with a microplate reader (μQuant, BioTek®, Winooski, VT, USA) and the protein amount was determined using the calibration curve constructed with bovine serum albumin. The amount of BSA adsorbed on the CLN was calculated by Equation 8:

$$q_e = \frac{[(C_i - C_e)\ x\ V]}{m} \quad (8)$$

where, q_e represents the amount of the BSA adsorbed by CLN in mg BSA/g CLN, C_i is the initial concentration of BSA, C_e is the concentration of BSA in the supernatant, V is the volume of BSA solution (L) and m is the weight of the CLN (g).

2.2.3. Preparation and Characterization of CLN/PCEC Composite Scaffolds

2.2.3.1. Preparation of Scaffolds

Highly porous CLN/PCEC composite scaffolds were produced through powder compression followed by particulate leaching (Figure 11). Briefly, pre-determined amount of PCEC copolymer was powdered in absolute ethanol by mixing at 2000 rpm for an hour (T25 Ultra-Turrax, IKA, China). Then, copolymer powder dried overnight in atmospheric oven was sieved through 50 μm meshes along with CLN and porogen ($NaHCO_3$). In order to produce a homogenous mixture, components were blended in absolute ethanol with stirring at 1000 rpm for 10 min. The blend was then poured into a glass petri dish and partially dried to form slurry to prevent the sedimentation of CLN and $NaHCO_3$ while drying. To remove ethanol, blend was dried in atmospheric oven for 24 h. After that, powder blend was put into stainless steel mold (13 mm in diameter) conditioned at 50°C and compressed under 250 MPa between relaxation supports for 3 min using cold press piston (Carver AutoPellet Press, IN, USA). Scaffolds with different amounts of CLN and different polymer-to-$NaHCO_3$ ratios

were prepared as given in Table 4. Fabricated scaffolds were in disc form with a diameter of 13 mm and a height of 4 mm.

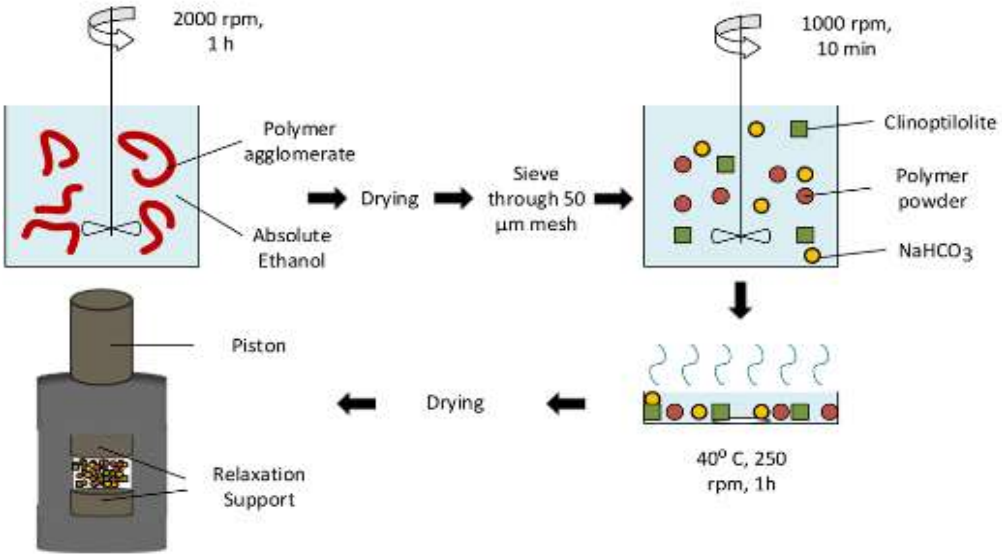

Figure 11. Preparation of CLN/PCEC scaffolds.

The prepared nonporous scaffolds were then put into dH_2O to remove $NaHCO_3$ to obtain porosity. At certain time intervals, water was refreshed and pH of the water was measured. A pH value of 7.00 was considered as the indication that $NaHCO_3$ leached out of the scaffolds. Obtained scaffolds were dried and stored at 4°C in a desiccator until use. As control groups, pure PCEC scaffolds were also prepared by using the same method.

Table 4. The amount of scaffold components for the preparation of CLN/PCEC composite scaffolds.

Scaffold Group *	Scaffold Annotation **	PCEC (mg)	CLN (mg)	$NaHCO_3$ (mg)
1:1	1:1	250	0	250
	1:1+10%	250	25	250
	1:1+20%	250	50	250
1:2	1:2	250	0	500
	1:2+10%	250	25	500
	1:2+20%	250	50	500

* Scaffold groups were according to the PCEC:$NaHCO_3$ weight ratio.

** Scaffolds were annotated according to CLN content as; none, 10% and 20% of PCEC content (w/w).

2.2.3.2. Determination of Reproducibility of the Technique

Solvent free fabrication method of scaffolds was tested for its reproducibility by determining the difference between the weights of the scaffolds prepared in different batches (n=7; two different sets in various time periods) and M_n value of copolymer (n=2) before and after preparation. The change in weights of the scaffolds before and after $NaHCO_3$ leaching was calculated gravimetrically as the percent change using Equation 9:

$$Weight\ Change\ (\%) = \frac{initial\ weight\ of\ scaffolds}{final\ weight\ of\ scaffolds} x100\% \quad (9)$$

The change in the M_n value of the copolymer before and after scaffold preparation was examined by using ^{1}H NMR spectroscopy. Additionally, the CLN content of scaffolds was determined by using TGA at a heating rate of 10°C/min between 30°C to 600°C. For all tests, pure porous PCEC scaffolds were used as control groups.

2.2.3.3. Scaffold Morphology

The surface morphology of CLN/PCEC scaffolds was examined by SEM (NanoSEM 430, FEI, OR, USA). Scaffolds were mounted onto metal stubs using carbon tape and vacuum-coated with gold (25 nm) by using Hummle VII sputter coating device (Anatech, Alexandria, VA, USA) before SEM analysis.

2.2.3.4. Porosity Determination

The porosity of the scaffolds was measured using Archimedes' Principle by applying liquid displacement method at room temperature (Olad & Farshi Azhar, 2014). A density bottle was filled with absolute ethanol as displacing liquid at 25°C since it is non-solvent for PCEC copolymer. Briefly, scaffolds were immersed into absolute ethanol with a predetermined volume of V_1 and cyclic pressurizing-depressurizing protocol was applied to force ethanol to move into the pores. The total volume of ethanol and completely sunk scaffold was indicated as V_2. After the scaffold saturated with ethanol was removed, the residual volume (V_3) was measured. Open porosity (ε) values of the scaffolds were calculated by using Equation 10:

$$\varepsilon = \frac{(V_1 - V_3)}{(V_2 - V_3)} \text{x} 100 \tag{10}$$

2.2.3.5. In vitro Degradation and Water Uptake Study

Degradation study for CLN/PCEC and pure PCEC scaffolds was conducted in 10 mL PBS solution (0.01 M, pH 7.4) in a shaking water bath at 37°C for 8 weeks (n=3). PBS solution was renewed every 2 days. Percent change in the weight of scaffolds after different incubation periods was evaluated using the Equation 11:

$$\%\, Weight\ Loss = \frac{M_i - M_f}{M_i}\ x\ 100 \tag{11}$$

where M_i and M_f represent the weight of the scaffolds before and after different incubation periods, respectively.

The water uptake behavior of the scaffolds at specific time intervals (1, 3, 6, 24, 48, 72, 96 and 120 h) was studied in 10 mL PBS solution (n=3). The wet weights of the scaffolds were measured at different incubation times. Before weighing the wet scaffolds excess water on the scaffolds was removed by blotting with filter paper. The

percent water uptake ratio of the scaffolds was calculated by using the Equation 12 where W_w stands for wet weight of scaffold at the given incubation period and W_i stands for the initial dry weight:

$$Swelling\ (\%) = \frac{W_w - W_i}{W_i} x100 \quad (12)$$

2.2.3.6. Mechanical Testing

The compressive strengths and moduli of the scaffolds were determined by universal testing machine (LR50 K Lloyd Instruments, UK) with a 50 kN load cell at a crosshead speed of 0.1 mm/min and the data were recorded using computer software (Nexygen MT; Ametek Inc., UK). The compression test was employed until 10% strain was achieved and the compressive modulus was calculated from the initial elastic region of the stress–strain curves obtained from the compression tests.

2.2.3.7. In vitro Bioactivity Analysis

Bioactivity of the scaffolds was evaluated by incubating the scaffolds in simulated body fluid (SBF, pH 7.4) prepared according to the Kokubo's method (Kokubo & Takadama, 2006). Scaffolds were placed in SBF containing smooth polypropylene beakers and incubated for 3, 7, 14 and 21 days at 37°C (n=5). SBF solution was refreshed every 2 days. At the end of each incubation period, the scaffolds were immediately rinsed with dH_2O and vacuum-dried for 24 h until a constant weight was achieved. Scaffolds were examined by SEM for mineralization. The Ca/P ratio and elemental composition of CaP formed on scaffolds were also evaluated by using the ratio of Ca and P peak intensities obtained in the EDS spectra.

2.2.3.8. In vitro Protein Adsorption on Scaffolds

In order to characterize in vitro protein adsorption capability, CLN/PCEC and pure PCEC scaffolds were incubated in 2 mg/mL FBS solution (diluted 30 times with 0.1 M PBS) (n=5). Briefly, scaffolds were sterilized with immersion in 70% (v/v) ethanol solution overnight and they were then thoroughly rinsed 3 times with 0.1 M PBS solution. Scaffolds were then pre-wetted overnight in 0.1 M PBS at 37°C and subsequently they were incubated in FBS solution for 24 h in a shaking water bath set at 150 rpm at 37°C. Scaffolds were removed from the FBS solution and rinsed with 1

mL PBS. Finally, scaffolds were incubated with 1 mL 1% SDS solution for 1 h and rinsed with PBS. The amount of weakly adsorbed protein was determined from the aliquots taken from PBS used in rinsing step whereas the amount of strongly adsorbed protein on the scaffolds was determined from the aliquots taken from SDS solution used for detaching proteins from scaffolds. Additionally, total protein in FBS was also determined prior to protein adsorption study. Briefly, 100 µL sample aliquots from various dilutions of FBS in PBS were taken and incubated with 800 µL BCA working solution at 60°C for 15 min. The amount of protein in the aliquots was determined by measuring the absorbance at 562 nm with a microplate reader. The amount of protein loadings were evaluated by using Equation 13:

$$Protein\ Adsorption = \frac{weight\ of\ protein\ adsorbed\ by\ scaffold}{weight\ of\ scaffold} x100 \qquad (13)$$

2.2.3.9. In vitro Studies

For cell culture studies, human fetal osteoblast (hFOB, 1.19) cell line (ATCC No.: CRL-11372) was used and cells were cultured in growth medium composed of Dulbecco's MEM/F-12 nutrient medium supplemented with 10% (v/v) FBS and 100 units/mL penicillin/streptomycin at 37°C in 5% CO_2 atmosphere in carbon dioxide incubator (5215 Shel Lab., Cornelius, OR, USA). After reaching 80% confluency, cells were subcultured by using 0.1% Trypsin/EDTA solution. Cells at 3rd passage were used in the experiments.

Prior to *in vitro* cell culture studies, scaffolds were sterilized by incubating in 70% (v/v) ethanol in dH_2O for 2 hours under cyclic pressurization-depressurization atmosphere and irradiation with UV for 30 min.

2.2.3.9.1. Analysis of Cell Viability and Proliferation

Metabolic activity of cells on the scaffolds was evaluated using Prestoblue® Cell Viability Reagent (Invitrogen, USA). Briefly, sterilized scaffolds were placed in the center of 12 well tissue culture plates and pre-wetted with 0.1 M PBS for 1 h prior to cell seeding (n=8). Cells were seeded at a density of 2 x 10^4 cells/scaffold in 25 µL volume and allowed for 30 min to attach. After seeding, scaffolds were incubated in

growth medium for 3 days. Cell culture medium was then replaced with osteogenic differentiation medium (Dulbecco's MEM/F-12 nutrient medium supplemented with 10% (v/v) FBS, 100 units/mL penicillin/streptomycin, 50 μg/mL ascorbic acid, 10 mM β-glycerophosphate and 10^{-8} M dexamethasone). Cells were further incubated for 14 days. Osteogenic differentiation medium was renewed every 2 days. At each time point, culture media were removed and a 1:9 ratio Presto Blue in growth media was added to each well. After incubation at 37ºC for 6 h, media were collected and their absorbance was read with a microplate reader (μQuant, BioTek®, Winooski, VT, USA) at 570 nm primary and 600 nm reference wavelengths. Cell-free scaffolds served as negative control. The calibration curve for metabolic activity was constructed with different number of cells (0 - 20 x 10^4 cells) to determine the average reduction of Prestoblue by hFOB cells on the scaffolds at various incubation periods. Shortly, after seeding different number of cells on TCPS and incubating for 6h for allowing cells to attach, Prestoblue® Cell Viability assay was conducted to determine percent reduction, as indicated in the assay kit and a calibration curve was constructed using % reduction data versus known cell number. Furthermore, average cell numbers on scaffolds after 1st and 2nd weeks of incubation were determined using DNA quantification analysis. Briefly, scaffolds were rinsed twice with PBS and incubated with a lysis solution consisting 0.1% (v/v) Triton X-100, sodium azide and PBS. Then, cellular lysates were combined with 1X TNE buffer (1:1 (v/v)) (Appendix E). Into this mixture, Hoechst DNA dye prepared in 1X TNE buffer was introduced to interact and produce UV fluorescence in accordance with the DNA concentration (Appendix E). The calibration curve of the dye against various concentrations of DNA were constructed using calf thymus serum (Appendix F).

To study the morphology of cells on scaffolds SEM analysis was done at the end of different incubation periods. Scaffolds were washed 3 times with PBS and cells were fixed with 4% paraformaldehyde for 1 h at room temperature. Then, scaffolds were rinsed 3 times with PBS and air-dried. After that, they were immersed in hexamethyldisilazane and dried before coating with gold (25 nm).

2.2.3.9.2. Analysis of Osteogenic Differentiation

To examine osteogenic differentiation of hFOB cells seeded on scaffolds, ALP activity assay (n=4), osteopontin (OSP) assay (n=3) and intracellular calcium quantification assay (n=4) were conducted. Cell-free scaffolds served as negative controls.

hFOB cells are osteoblast-lineage cells showing primary cellular properties such as proliferation, extracellular matrix (ECM) production and differentiation into mature phenotype (Setzer et al., 2009). Directly related with aforementioned properties of hFOB, these cells were selected for complete analysis of biological responses to BTE scaffolds produced throughout the study.

Briefly, hFOB cells were seeded on scaffolds at a density of 2×10^5 cells/scaffold in 25 µL aliquots and they were incubated in osteogenic differentiation medium for various time intervals (7, 14, 21 and 28 days). The culture media were changed every second day. At the end of each time point, collected scaffolds were washed three times with PBS and subsequently incubated with cell lysis buffer provided with ALP detection kit to determine the ALP activity of cells. Cell lysates were collected and centrifuged at 13000 rpm for 3 min. 80 µL aliquots were taken from each sample and incubated with para-nitrophenyl phosphate substrate in the dark for 1 h. Then, 50 µL stop solution was added and the optical density was measured at wavelength of 405 nm using microplate reader (µQuant, BioTek®, Winooski, VT, USA). Protein contents of the lysates were determined with µBCA assay using the calibration curve constructed with different concentrations of BSA. The enzyme activity of cells was given in terms of specific enzyme activity (nmol/mg protein/min).

OSP secretion by the cells was used as a late stage marker of osteogenic differentiation of cells. In order to determine the cumulative release of OSP, media were collected during media changes and stored at -80^{o}C until analysis. The OSP level of each group was determined at the end of each week by using OSP detection kit. Optical density of the final product solutions was measured at 450 nm with microplate reader.

Furthermore, calcium amounts deposited by the cells were determined in the cell lysates using o-cresopthalein assay (Nuttelman et al., 2005). 10 µL aliquots of cell lysates were incubated in 0.1 M HCl overnight. Obtained solution was mixed with 200 µL o-cresopthalein and 8-hydroxyquinone-5-sulfonic acid in 2-amino-2-methyl-1,3 propanediol to form complex with intracellular calcium. The intensity of the color was measured at 560 nm using microplate reader.

2.2.4. Statistical Analysis

One way analysis of variance (ANOVA) with Tukey's post hoc test for multiple comparisons using SPSS software (ver. 23.0; IBM Corporation, NY, USA) was used for the statistical analysis of the data. Differences were considered significant at $p \leq 0.01$. The results are expressed as mean ± standard deviation (SD).

CHAPTER 3

RESULTS

3.1. PCEC Triblock Copolymer Characterization

In the FT-IR spectrum of PCEC triblock copolymer, characteristic FT-IR peaks of both PCL and PEG segments were observed (Figure 12A). Typical peaks of PCL segments can be observed at 1719 cm^{-1} due to weak C=O vibrations at ester carbonyl group of the repeated PCL units and at 1237 cm^{-1} due to -COO- vibrations. The absorption bands at 2943 cm^{-1} and 2865 cm^{-1} were attributed to the symmetric and asymmetric -CH_2- stretching vibrations of homosequences of the PCL units, respectively. Furthermore, PEG units within the PCEC copolymer were observed as characteristic absorption bands at 1162 cm^{-1} due to -C-O-C- stretching in the -OCH_2CH_2- repeated units.

The formation of the PCEC triblock copolymer was verified using ^{1}H NMR spectroscopy. Both of the characteristic proton peaks of PCL and PEG units were observed in the spectrum of PCEC copolymer (Figure 12B). The presence of PCL unit was confirmed with the peaks observed at 1.40 - 1.65 ppm, 2.32 and 4.07 ppm for the protons of -$(CH_2)_3$-, -$OCCH_2$- and –CH_2OOC- groups, respectively. Singlet band observed around 3.65 ppm confirmed the presence of PEG homosequence units within the structure. Moreover, a weak peak observed in 4.23 ppm was attributed to the methylene end groups of the PEG homosequence linked to PCL homosequences.

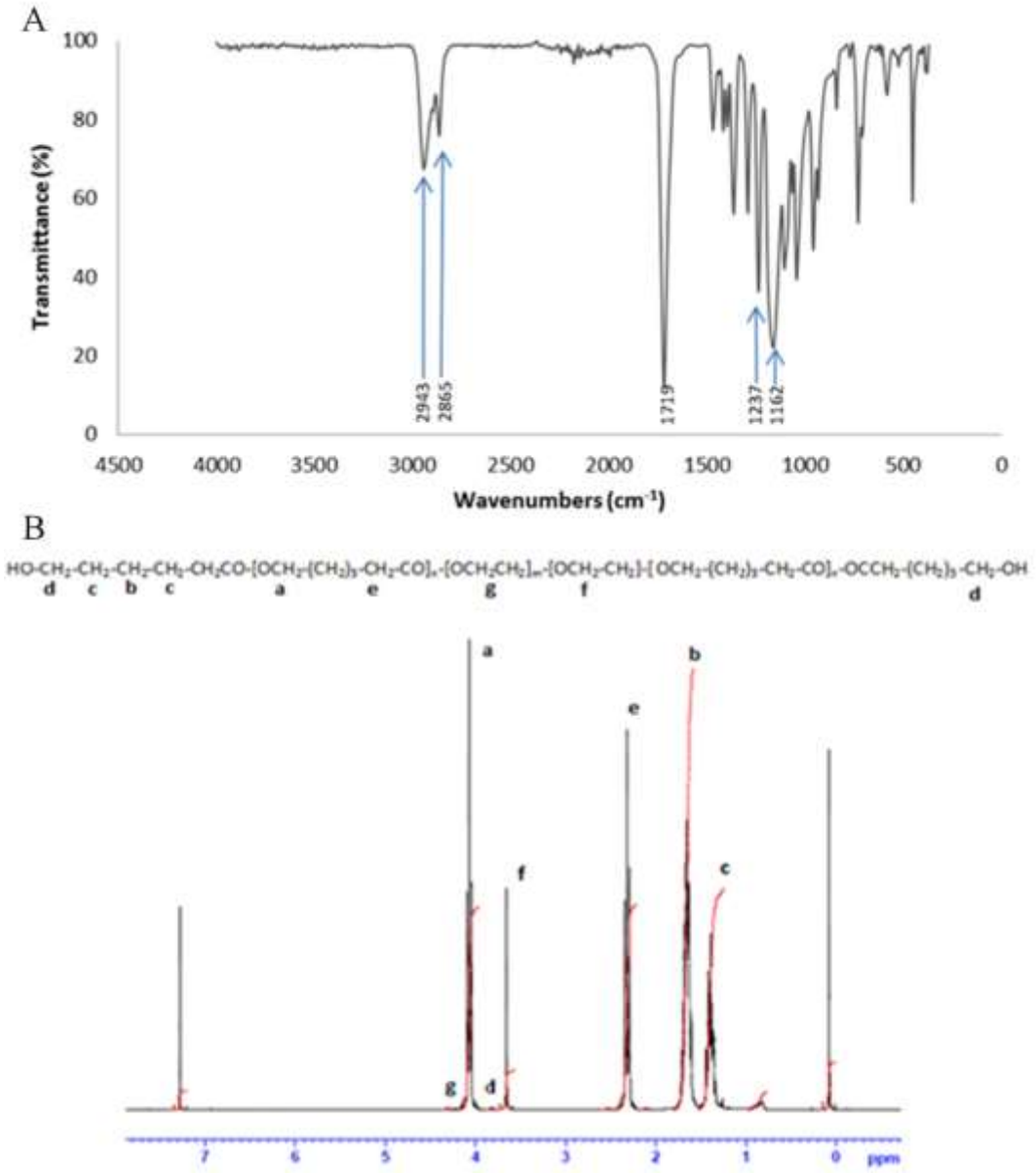

Figure 12. FT-IR (A) and 1H NMR (B) spectra of PCEC.

All theoretical and experimental ([ε-CL]/[EG]) monomer ratios and number average molecular weight (M_n) of the synthesized copolymer are given in Table 5. M_n value of the copolymer was calculated in two different ways based on the initial feed concentration ratios and integrity ratio of the ^{1}H NMR peaks at 4.07 ppm to methylene protons (-CH_2-) of PCL segment and 3.65 ppm (-CH_2-) to PEG segments by using equations given as supplementary information (Appendix H).

Table 5. Number average molecular weight of the synthesized PCEC triblock copolymer.

Polymer	**[ε-CL]/[EG]***	**[ε-CL]/[EG]****	**Mn*** (kDa)**
PCEC	9.25/1	5.25/1	58

* Initial feed concentration ratio for the polymerization reaction.

** PCL to PEG ratio was calculated from corresponding ^{1}H NMR peaks.

*** M_n value calculated based on the integrity ratio of the ^{1}H NMR peaks at 4.07 ppm to methylene protons (-CH_2-) of PCL segment and 3.65 ppm (-CH_2-) to PEG segments.

Thermal properties of the PEG and PCL homopolymers and PCEC triblock copolymer are presented in Table 6. Crystallinity (X_c value) of the copolymer was found close to that of PCL homopolymer. PCL and PEG (X_{cPCL} and X_{cPEG}) homosequence crystallinity in PCEC copolymer was altered. X_{cPCL} increased while X_{cPEG} decreased. For PCEC copolymer, two T_d values attributed to PCL and PEG units were observed, which confirmed the block copolymer structure.

Table 6. Thermal properties of PCL and PEG homopolymers and PCEC triblock copolymer determined with DSC and TGA

Polymer	T_m (^{0}C)	T_c (^{0}C)	ΔH_m1 * (J/g)	ΔH_m2 ** (J/g)	X_c *** (^{0}C)	T_d (^{0}C)
PCL	60.10	40.65	95.39	139.5	68	290
PEG	61.66	44.75	171.71	189.8	90	320
PCEC	62.38	36.41	98.66	-	70 (71 and 51)	280 and 325

* The enthalpy of melting obtained in DSC analysis for each homopolymer and copolymer.

** The enthalpy of melting of 100% crystalline homopolymer (theoretical value).

*** Percent crystallinity, PCEC triblock copolymer was calculated using M_n and ΔH_m values of homopolymers.

3.2. CLN Characterization

The general morphology of the CLN particles is given in Figure 13A, B and C. CLN particles had flake-like structures and agglomerations of smaller particles. Zeta potentials of CLN at various pH values are shown in Figure 13D. The isoelectric point (IEP) of the CLN mineral was observed at pH 4.65. The CLN particles had negative surface charge in the neutral zone (pH 7.00) (Figure 13D). EDS spectrum of the pure CLN showed the presence of Si, Al, Mg, Ca, K and O elements in its structure (Figure 13E). The particle diameter distribution of CLN and the SPAN value are given in Figure 13F.

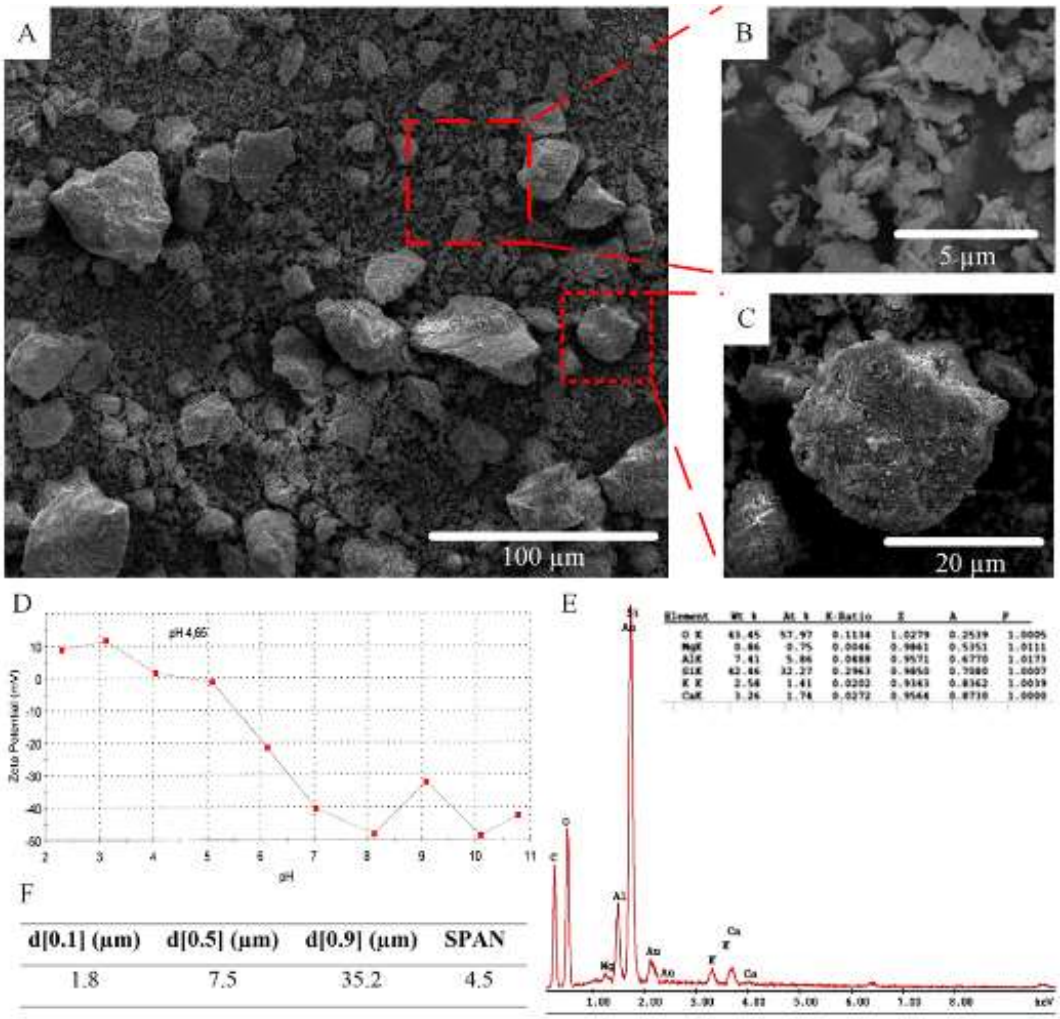

d[0.1] (µm)	d[0.5] (µm)	d[0.9] (µm)	SPAN
1.8	7.5	35.2	4.5

Figure 13. Characteristics of the CLN particles: (A) – (C) SEM images of CLN particles: general view of particles (A) and view of flake-like particles (B) as well as agglomerations (C) at higher magnifications. (D) Zeta potential of CLN as a function of pH between 2 and 11. (E) Elemental composition of the CLN. (F) Undersized particle percentiles and calculated SPAN value for CLN.

CLN was also analyzed for structural composition. XRD study on CLN verified that the mineral possessed unique intensities at specificied theta angles as standard CLN (JCPDS No: 025-1349, Figure 14).

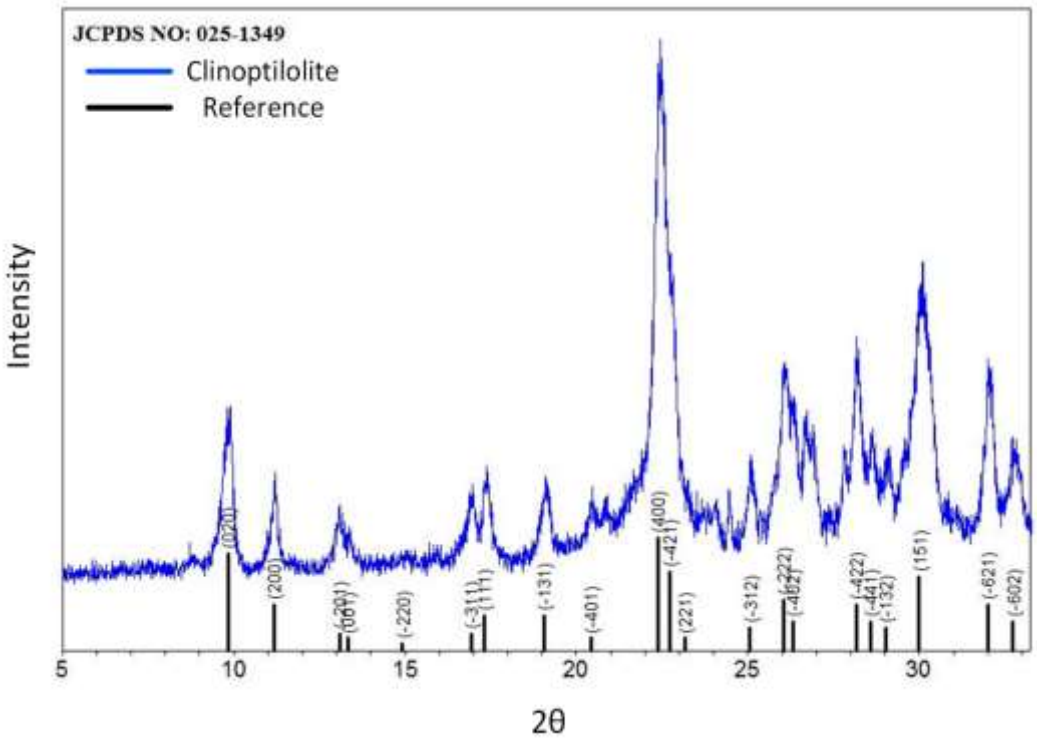

Figure 14. XRD of CLN and standard (JCPDS No: 025-1349).

Protein adsorption characteristic of CLN was investigated in NaCl solutions at different ionic strengths (0.05, 0.1 and 0.15 M NaCl solutions) at 37°C (Figure 15). During 24 h incubation, an increase in the cumulative amount of protein adsorption on CLN was observed for all ionic strengths (Figure 15A). Although there was no significant difference between the adsorption isotherms observed at different ionic strengths, CLN showed highest protein adsorption capacity in 0.1 M NaCl solution (Figure 15B).

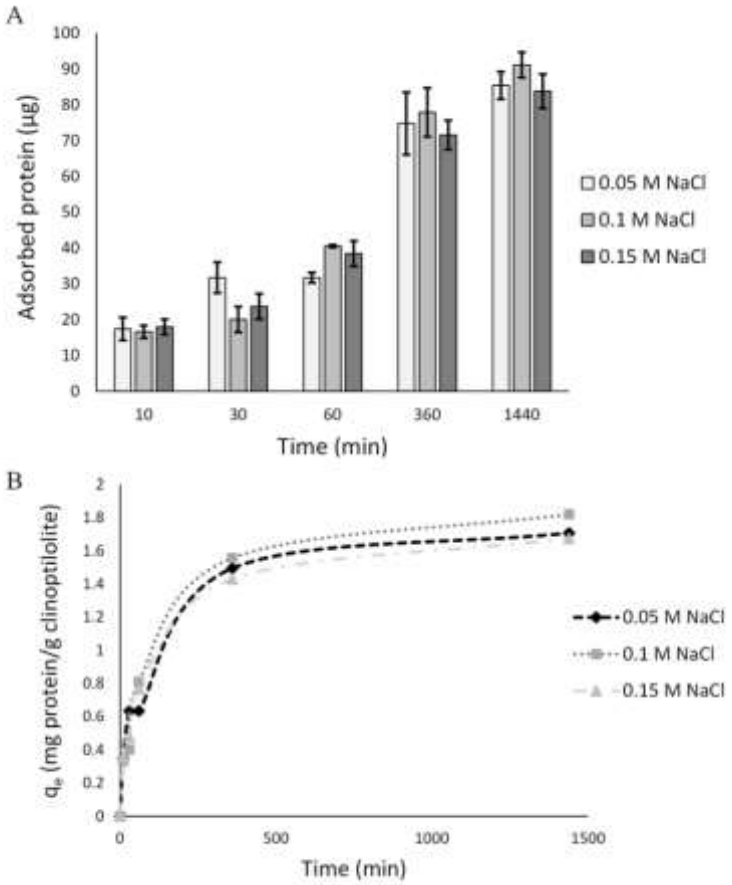

Figure 15. Total protein adsorbed on CLN (A) and adsorption isotherms of BSA on CLN (B) incubated in NaCl of different ionic strengths at 37°C. No significant difference was observed between groups ($p<0.01$).

3.3. Scaffold Characterization

3.3.1. Determination of Reproducibility of the Technique

No significant difference in the M_n values was observed between the starting PCEC triblock copolymer (58 kDa) and their processed forms in scaffolds (Table 7). Moreover, experimental percent weight changes of scaffolds after $NaHCO_3$ leaching was found close to the theoretical values of their counterparts in each group (Table 7). Amount of CLN content in scaffolds (PCEC:NaHCO3+CLN%; 1:1+10% and 1:1+20%) was found close to respective theoretical contents (Table 7).

Table 7. Theoretical and experimental percent weight changes of scaffolds after $NaHCO_3$ removal.

Scaffold	Theoretical Weight Change (%)	Experimental Weight Change (%)	Theoretical CLN Content (%)	Experimental CLN Content (%)	M_n of PCEC in Scaffolds (kDa)
1:1	-50.00	-50.46 ± 1.99	0	0	51 ± 4
1:2	-66.67	-66.75 ± 0.97	0	0	53 ± 3
1:1+10%	-47.62	-45.87 ± 1.00	10	8.8	56 ± 3
1:1+20%	-42.86	-43.65 ± 2.50	20	16	56 ± 4
1:2+10%	-64.52	-60.25 ± 2.58	10	11	56 ± 3
1:2+20%	-62.50	-58.00 ± 3.42	20	16.5	56 ± 3

* Experimental data: mean ± SD; n=7 for weight change (%) and n=2 for M_n of triblock copolymer.

3.3.2. Morphology of Scaffolds

According to the cross-sectional SEM images of the scaffolds, presence of the CLN did not change overall morphology of the scaffolds (Figure 16). In all groups, wide pore size distributions were observed (Figure 16).

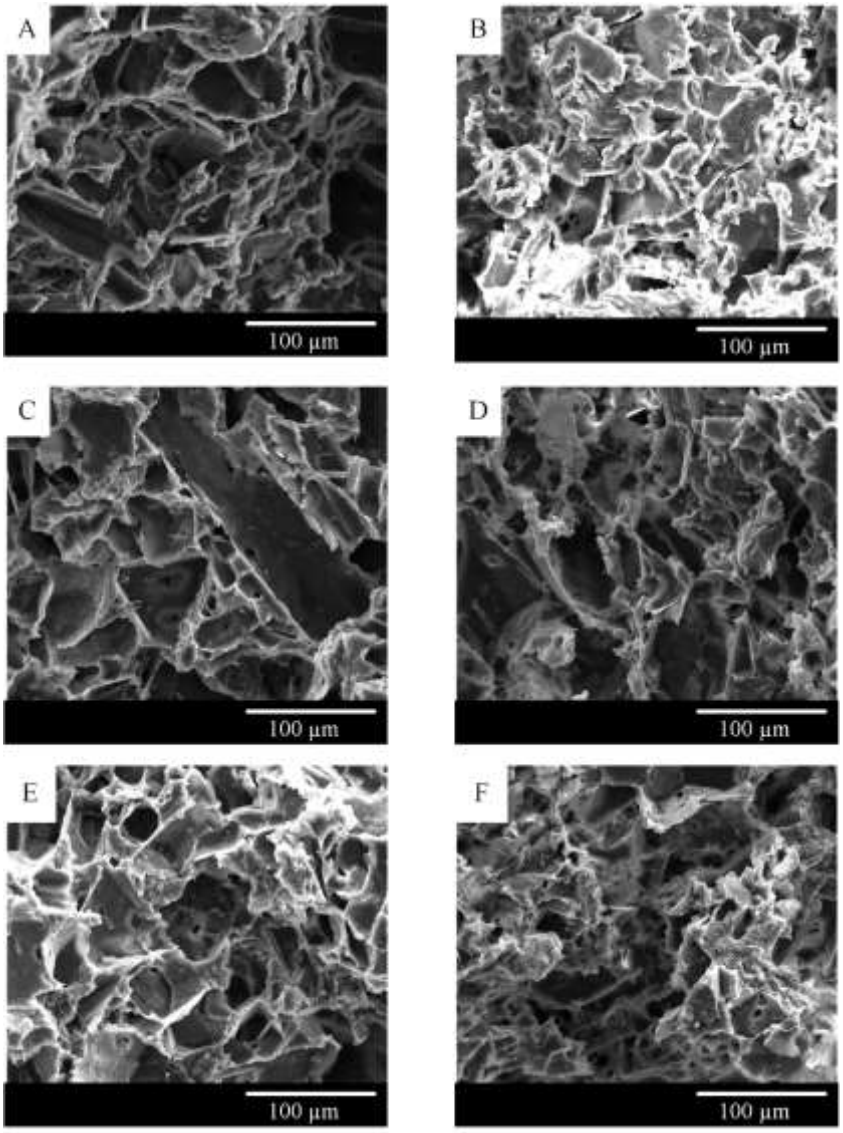

Figure 16. SEM images of scaffolds containing PCEC/ $NaHCO_3$ as (A) 1:1, (B) 1:2, and PCEC/$NaHCO_3$+Clin as (C) 1:1+10%, (E) 1:1+20% and (D) 1:2+10%, (F) 1:2+20%.

General photograph and detailed SEM images at different magnifications of the representative scaffold (PCEC:$NaHCO_3$+CLN%; 1:2+20%) are given in Figure 17. Hierarchical pore structure of scaffold was clearly observed in the cross-sectional images of the scaffold (Figure 17). Inside the scaffold, smaller pores were connected to larger pores through canals.

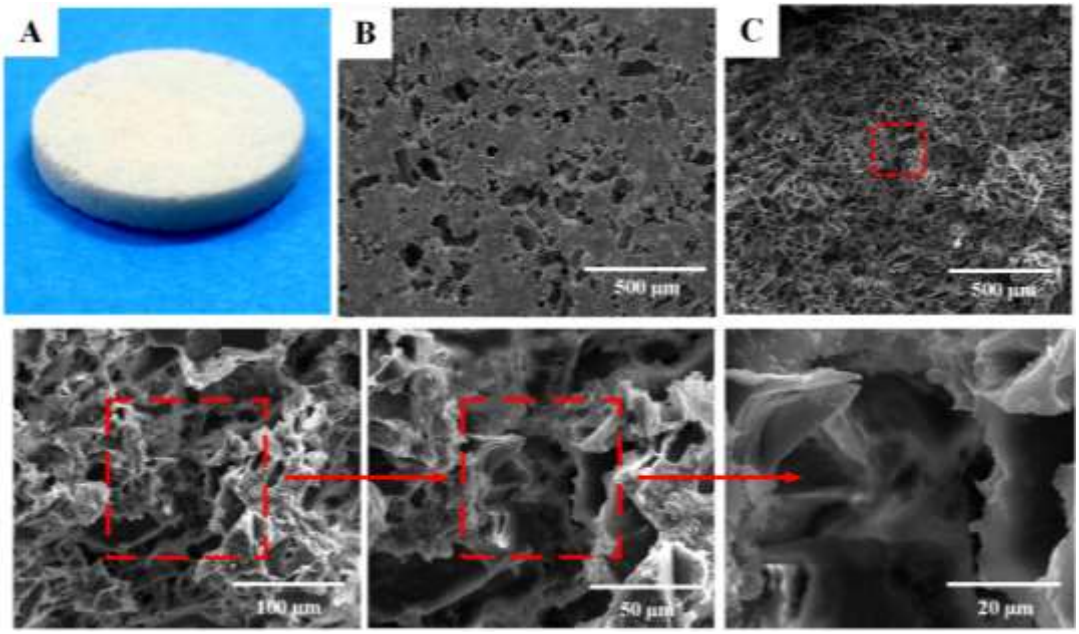

Figure 17. General photograph and hierarchical SEM images of representative scaffold, PCEC:$NaHCO_3$+CLN%; 1:2+20%: The general outlook of scaffold (A), surface pores (B) and hierarchical pore structure of scaffold with interconnective macropores with canals and micropores at their walls when focused on the area designated in cross-sectional view (C).

3.3.3. *In Vitro* Degradation and Water uptake Study

At the end of degradation study, no significant change in the structural integrity and weights of pure PCEC and CLN/PCEC scaffolds was observed (data not shown). According to the results of water uptake study, 1:2 (PCEC:$NaHCO_3$) scaffold groups containing different amounts of CLN showed higher water uptake compared to their 1:1 counterparts (Figure 18).

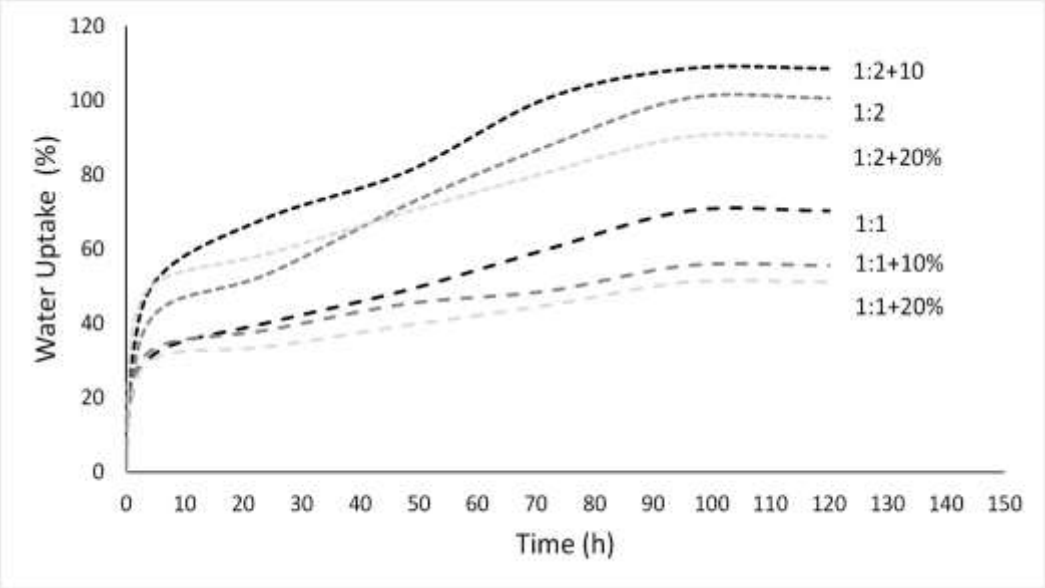

Figure 18. Water uptake properties of the pure PCEC and CLN/PCEC scaffolds. In water uptake study, scaffolds (1:1) are significantly different than scaffolds (1:2).

3.3.4. Mechanical Properties and Porosity of Scaffolds

Pure PCEC and CLN/PCEC scaffolds were mechanically tested up to 10% strain where their 3D structure yielded. Compressive stress-strain curves of the scaffolds and comparison of their compressive moduli and total open porosity are given in Figure 19. Scaffold group having 1:1, PCEC:$NaHCO_3$ ratio showed higher compressive strength and modulus compared to the other groups (Figure 19A and B). Moreover, scaffolds with higher CLN content provided better mechanical properties under compression than that of scaffolds with lower CLN content. The compressive moduli was also higher for 1:1 groups than those of 1:2 groups which had higher open porosity as presented in Figure 19B.

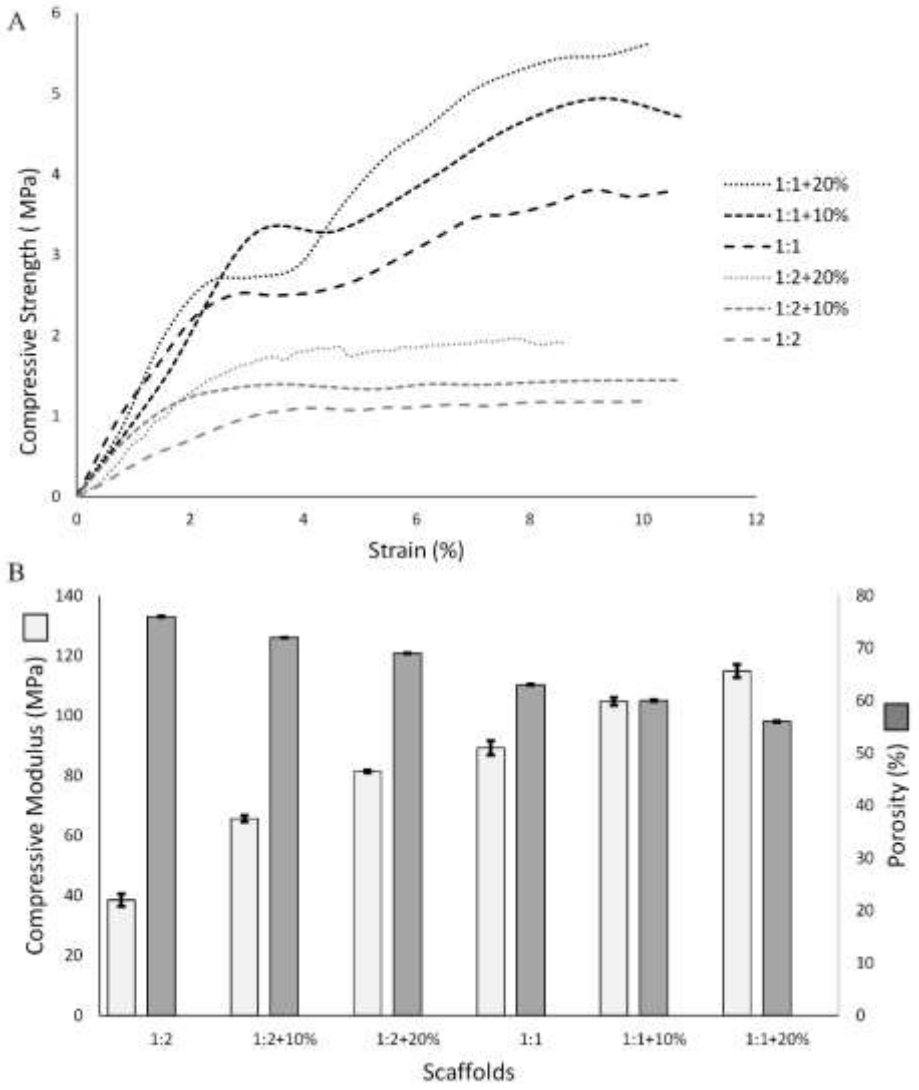

Figure 19. Compressive stress-strain curves of the scaffolds (n=3) (A) and compressive moduli and total open porosity of the scaffolds (n=3) (B). Scaffold groups (1:1 and 1:2) were significantly different ($p<0.01$).

The scaffold group having 1:1 PCEC/$NaHCO_3$ ratio (namely 1:1, 1:1+10% and 1:1+20%) was selected for further studies according to mechanical, chemical and physical properties of the scaffolds such as compressive strength, modulus, water uptake, and overall porosity.

3.3.5. Protein Adsorption on Scaffolds

The total amount of serum proteins that were strongly and weakly adsorbed on the scaffolds are given in Figure 20A. Higher amount of protein was adsorbed on the scaffolds containing highest CLN content (1:1+20%) compared to that adsorbed on pure PCEC scaffolds and scaffold with lower CLN content. Conversely, the amount of protein weakly adsorbed on the pure PCEC scaffold was higher compared to the scaffolds containing CLN.

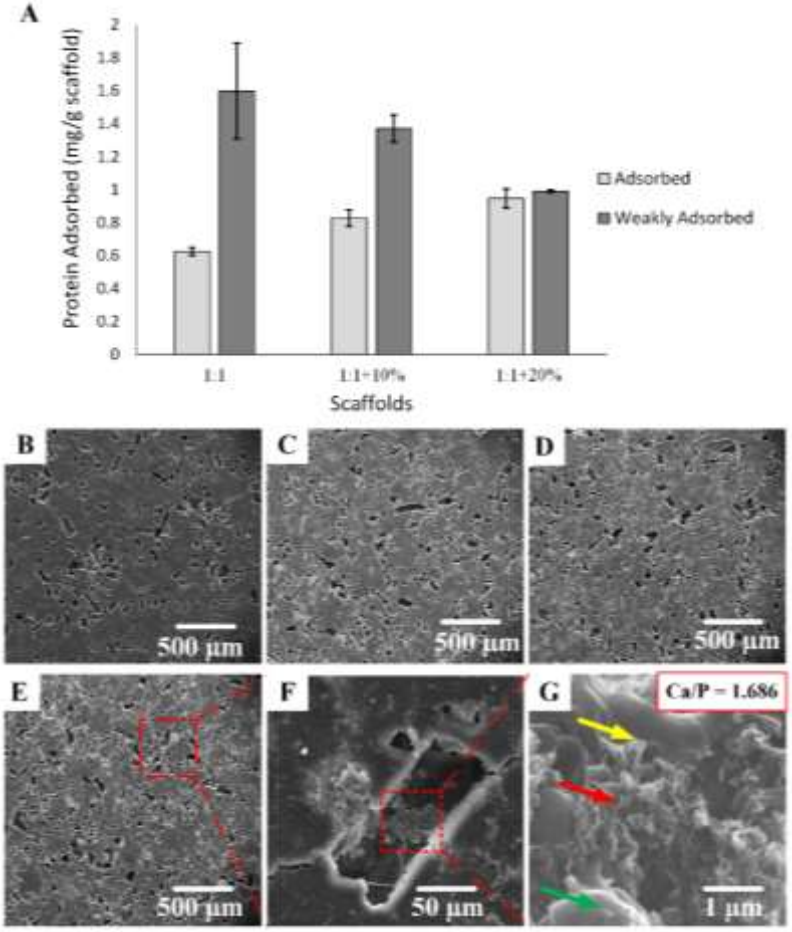

Figure 20. Total amount of strongly and weakly adsorbed serum proteins on scaffolds as a ratio of mg protein/g scaffold (A) (Significantly higher protein adsorption was observed with 1:1+20% than all other scaffolds). SEM images of the scaffolds after immersion in SBF for different time periods: (B-D) general views of the 1:1, 1:1+10% and 1:1+20% scaffolds after 3 days of SBF immersion, respectively, (E) general view of 1:1+20% scaffold after 14 days of SBF immersion, (F) CaP precipitation in pore of 1:1+20% scaffold after 14 days of SBF immersion and (G) apatite formation around the CLN content in the 1:1+20% scaffold after 14 days of SBF immersion. (Red arrow indicates apatite formation. Yellow arrow indicates CLN content and green arrow indicates copolymer content of the scaffolds).

3.3.6. *In Vitro* Bioactivity of Scaffolds

In order to evaluate the bioactivity of the scaffolds, they were immersed in SBF solution. After different incubation periods, scaffolds were examined by SEM to

investigate the CaP deposition (Figure 20B-G). CaP precipitation on the composite scaffolds (containing 10% and 20% CLN) was seen after 3 days of incubation (Figure 20B, C and D), whereas CaP precipitation on the pure PCEC scaffolds (1:1) was observed at the end of one week (data not shown). Moreover, SEM examination showed that 1:1+20% (PCEC:$NaHCO_3$+CLN%) scaffolds had higher CaP deposition both on surface and at the peripheries of the pores (Figure 20E and F). In addition, specific needle-like appearance of the HA was observed on the CLN containing scaffolds (Figure 20G). According to the results of EDS elemental analysis, the presence of Si, Al and Mg elements indicated the CLN content at CaP sites where the Ca/P ratio was found as 1.686, close to the ratio for bone apatite (Ca/P= 1.67).

3.3.7. *In Vitro* Studies

3.3.7.1. Cell Viability and Proliferation

The proliferation of hFOB cells on the scaffolds was monitored using a PrestoBlue cell viability assay, a resazurin based metabolic assay, for 14 days (Figure 21A). Average metabolic activity of hFOB cells on scaffolds showed a gradual increase during the first week; however a significant decrease in the average cell number was observed at the second week of incubation (Figure 21A). Furthermore, determination of hFOB DNA concentrations on scaffolds in first and second weeks showed that cell numbers increased for all groups while highest CLN containing group, 1:1+20% (PCEC:$NaHCO_3$+CLN%) scaffolds, displayed highest cell number throughout the incubation periods (Figure 21A). In addition, SEM image of hFOB cells on 1:1+20% (PCEC:$NaHCO_3$+CLN%) scaffold after 14 days of incubation is given in Figure 21B. Apatite depositions on the surface regions between cells were also confirmed by EDS elemental analysis (Figure 21B).

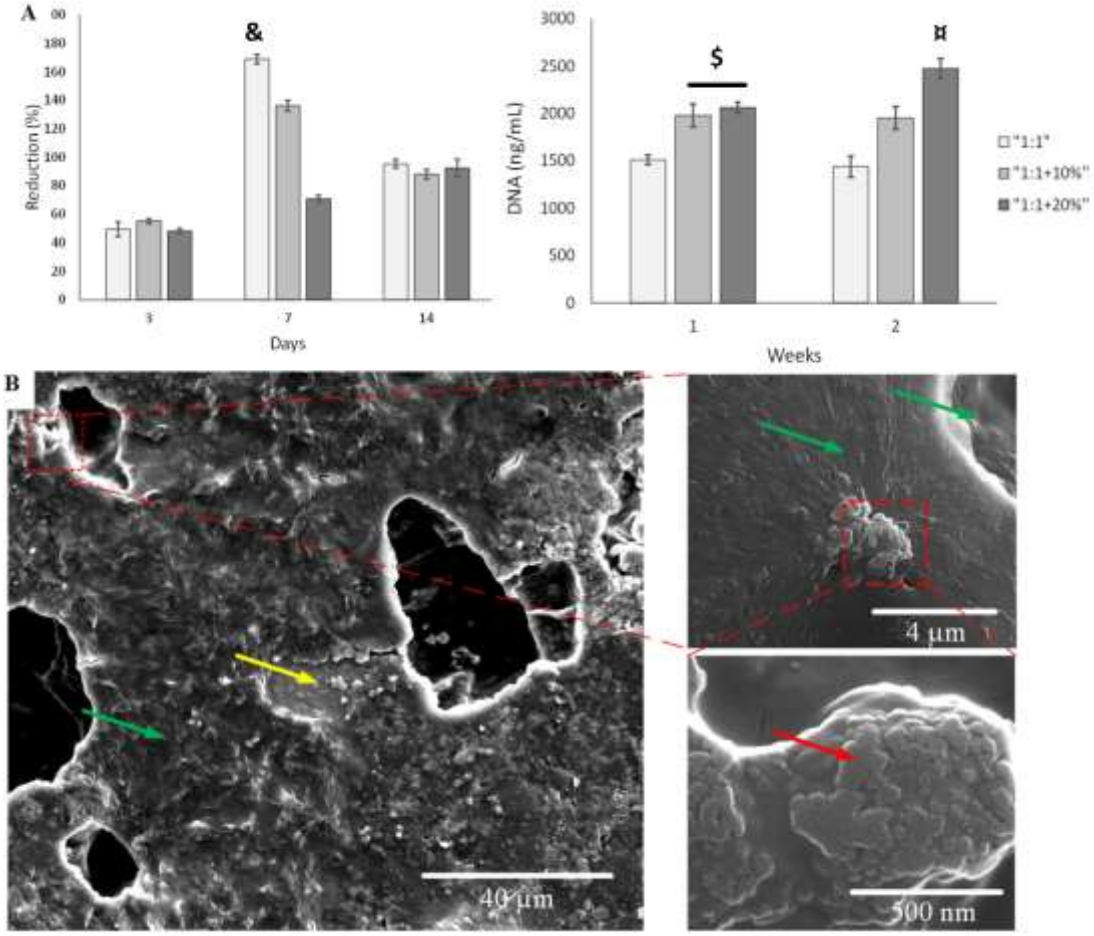

Figure 21. Average metabolic activity of hFOB cells present on the scaffolds determined with PrestoBlue® assay for 14 days (n=8) and average DNA concentration of hFOB cells on scaffolds were given (n=4) (A). SEM images of hFOB cells on the surface of 1:1+20% (PCEC:$NaHCO_3$+CLN%) scaffolds after 7 days post-seeding (B) (Red arrow: apatite formation, yellow arrow: surface of scaffolds, green arrow: confluent cell layer) (Significant differences are given as &: PCEC scaffold showed highest value, $: both CLN containing scaffolds showed highest and ¤: 1:1+20% scaffold showed highest value at given time ($p<0.01$).

3.3.7.2. Cellular Differentiation

High ALP activity was observed for hFOB cells seeded on all types of scaffolds until 3rd week (Figure 22A). However, at the end of 4th week, ALP activity of cells significantly decreased. Cells seeded on scaffolds containing CLN had higher ALP

activity compared to scaffold groups without CLN at the first week. hFOB cells seeded on 1:1+10% (PCEC:$NaHCO_3$+CLN%) scaffolds displayed highest ALP activity at the end of the first week.

The levels of OSP released by the cells increased in all groups during 4 weeks (Figure 22B). Highest OSP levels were obtained at the end of 4^{th} week in all groups. However, cells seeded on CLN containing scaffolds secreted higher OSP throughout the study. Calcium deposition by cells was found higher for hFOB cells seeded on CLN containing scaffolds for the first week when compared to PCEC scaffolds. Similar calcium amounts were found for all scaffold groups in the following weeks (Figure 22C). At the 4^{th} week, calcium deposition by the cells significantly decreased compared to 1^{st} week.

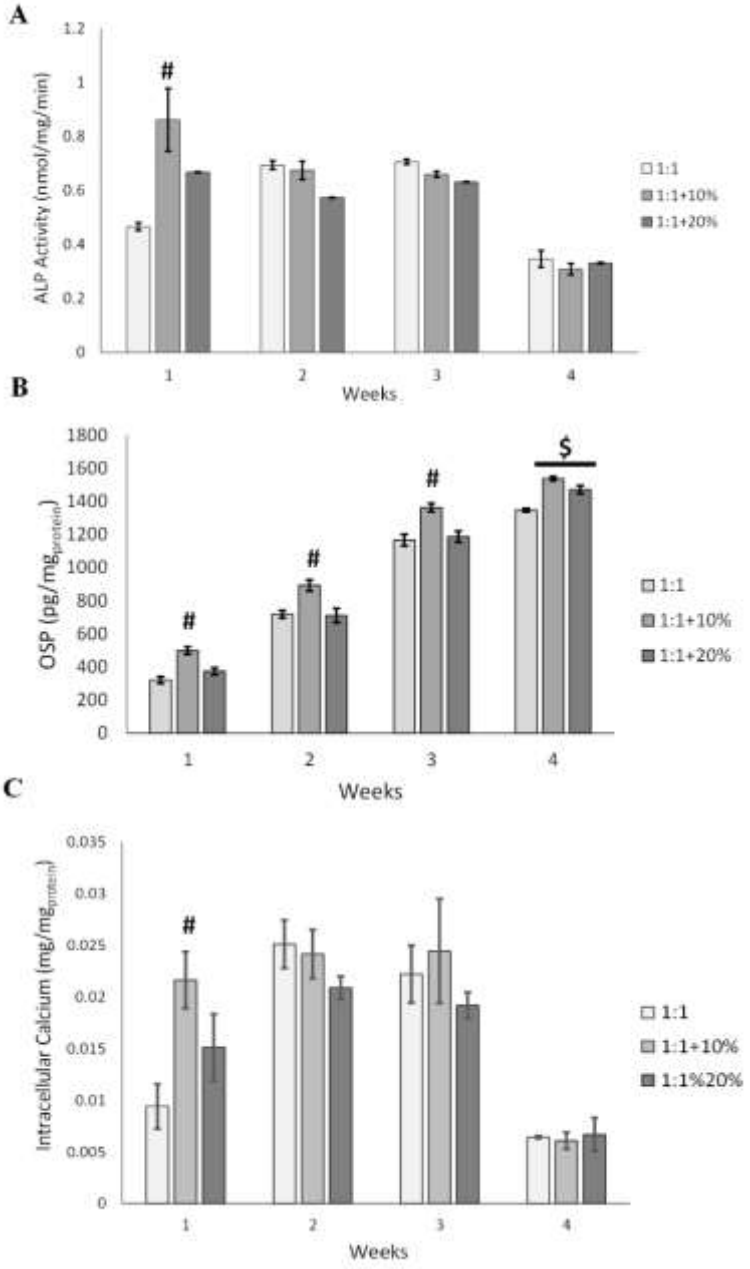

Figure 22. Average ALP activity (n=4) (A), cumulative OSP release (n=3) (B) and intracellular calcium content (n=4) (C) of hFOB cells seeded on pure PCEC and CLN/PCEC composite scaffolds having 1:1 PCEC/$NaHCO_3$ ratio. (Significant differences are given as #: 1:1+10% scaffolds showed significantly higher ALP, OSP and intracellular calcium concentrations compared to other groups at given time points and $: Both CLN containing groups were significantly larger than pure PCEC scaffolds, $p<0.01$).

CHAPTER 4

DISCUSSION

Polymer-mineral composite scaffolds have been extensively studied in BTE, which would provide the combination of desired unique properties of each of its components (Dhandayuthapani, 2011; Gloria et al., 2010). In literature solvent casting and melt-processing are among the widely used methods to produce polymer based composite bone scaffolds (Mouriño & Boccaccini, 2010; Shrivats et al., 2014). However, use of solvent in the production of the scaffolds causes a concern of biocompatibility for the possibility of residual solvent remaining in the scaffold (Y. Liu et al., 2013). Additionally, there is a very limited choice of polymers for melt processing due to the rheological issues (Aho et al., 2015). Therefore, alternative scaffolding methods, which avoid use of solvents and melt processing are still required.

For the production of 3D bone tissue scaffolds, controlling porosity and interconnectivity of the pores are important issues (Ozcelik et al., 2014). The cellular adhesion on scaffolds and subsequent penetration into the scaffolds depend on the pore sizes while interconnectivity promotes nutrient transport and waste product exchange, thus, tissue infiltration and efficient bone repair (Wagoner J. & Herschler, 2011). Particulate leaching technique is used to produce interconnective porous 3D constructs by porogen particles leaching out from the construct when soaked into appropriate solvent (Lim et al., 2008). In our study, CLN/PCEC triblock copolymer composite scaffolds were prepared by a reproducible method without the use of solvent and melting processing to prepare biocompatible, biodegradable, highly porous, interconnective and mechanically strong scaffolds for BTE.

4.1. Properties of Synthesized PCEC Copolymer

PCEC triblock copolymer was synthesized and characterized. Both of the characteristic FT-IR peaks of PCL and PEG segments were observed in the spectrum in accordance with literature (Figure 12A)(Feng et al., 2012; Gong et al., 2007). Additionally, ^{1}H NMR spectrum of PCEC triblock copolymer exhibited the characteristic ^{1}H chemical shift bands as reported in the previous studies (Figure 12B) (Du et al., 2007). Furthermore, the triblock copolymer formation was confirmed with the proton peak around 4.23 ppm coming from the hydrogens at the PCL and PEG linkage (Ma et al., 2010). According to the results of DSC, the percent crystallinity of the PCEC triblock copolymer was found close to that of PCL homopolymer (Table 6). T_m, T_c and ΔH_m values of PCEC copolymer were found higher than those of PCL homopolymer due to the presence of PCL segment with higher molecular weight in the copolymer structure in contrast to the PCL homopolymer (Zhou et al., 2003). Dahamaniya et al. (Dhamaniya et al., 2012) reported that increase in homosequence chain length of semicrystalline poly (lactic acid) in triblock copolymeric structure of PLA-b-PHIT-b-PLA resulted in increase of X_{cPLA}. Similarly, X_{cPCL} increment in the PCEC occurred after polymerization due to increase in homosequence chain length. Differential thermogravimetric curve of triblock copolymer showed two weight loss steps due to decomposition of PCL and PEG segments in copolymer (data not shown), which confirms the block copolymer structure (Hemmati et al., 2015). According to the comparison of the T_d values of copolymer and homopolymers, thermal stability of PCEC copolymer was higher than that of pure PCL and PEG homopolymers. In a similar study, Wang et al. (Yuelong Wang et al., 2013) studied PCEC block copolymer and found that increase in T_d of the blends was associated with increment in thermal stability.

4.2. Characterization of CLN

4.2.1. Particle Size and Morphology of CLN

Plate formations were observed for CLN of flake-like structures in the SEM analysis (Figure 13A-C). In another study, Ahmad et al. (Ahmad et al., 2012) showed that irregularly shaped HA particles contributed to compaction of both themselves and polyethylene matrix. Thus, irregular and different sized CLN particles were expected

to strengthen the mechanical interlocking with each other and also with copolymer PCEC matrix under compression during the preparation of CLN/PCEC composite scaffolds. As explained in another study, larger HA particles (50 μm) provide flow while small HA particles (4 μm) enable stronger packing (Will et al., 2008). Consequently, polydisperse particle size (1-50 μm) of CLN was thought to increase the compaction during powder compression.

4.2.2. Protein Adsorption Capacity of CLN

Protein adsorption capacity of the zeolites depends on the isoelectric point (IEP) of the proteins, chemical structure of the zeolites and pH of the environment (Kirdeciler et al., 2014; Krohn & Tsapatsis, 2005). To investigate the protein adsorption on the CLN particles, BSA was chosen as a model protein because of its net negative charge in neutral pH (Shi et al., 2005). CLN was finely dispersed and suspended in the BSA solution due to its good stability in neutral pH determined by zeta potential analysis. It was observed that CLN had basic species (OH^- ions) in a solution at pH 7.4 (Figure 13D) and CLN and BSA have IEP around pH 4.6 and 5.4, respectively. Although zeta potentials of the CLN and protein were found to be similar at neutral pH, BSA adsorption results (Figure 15A) showed that CLN could adsorb BSA at pH 7.4. CLN readily interacts with the environment due to its positively charged ions such as Mg^{2+}, Ca^{2+}, K^+ and it also has high ionic exchange ability at the surface due to its small Si/Al ratio (5.73), (Chiku et al., 2006; Tavolaro et al., 2007). Moreover, it was observed that ionic strength of the environment had no significant effect on the protein adsorption capacity of the CLN (Figure 15B). As studied in a previous study, protein adsorption on HA favors Langmuir kinetics (Bouropoulos & Moradian–Oldak, 2003). Thus, CLN might have generated a favorable adsorption surface for BSA and BSA adsorption on it obeyed the Langmuir kinetics.

4.3. Characterization of CLN/PCEC Composite Scaffolds Prepared with Solvent Free Powder Compression/Particulate Leaching Method Using $NaHCO_3$ as Porogen

4.3.1. Porosity of CLN/PCEC Composite Scaffolds

The morphology of the pores inside the scaffold may only depend on the overall shape and size of the $NaHCO_3$ particles and their agglomerations in the copolymer matrix. In addition, micropores (~1 um) were observed besides macropores (>100 um) demonstrating the interconnective porous structure of the scaffolds (Figure 17). Macropores in the scaffold structure provide larger surface area for cellular proliferation and tissue ingrowth at the implanted site (Gentile et al., 2012). Furthermore, microporous interpore openings between macropores provide better cellular attachment into the scaffolds while facilitating nutrient flow and waste removal (Pereira et al., 2012). Existence of pore size gradient in the scaffold structure is known to cause faster and better bone healing (Roy et al., 2003). Similarly, interconnectivity of the pores and high porosity in all scaffold groups provide large surface area, causing greater water uptake (Park et al., 2015). The porosity influences water uptake capacity of the scaffolds. Scaffolds having 1:2 (PCEC:$NaHCO_3$) ratio had higher porosity (Figure 19B) and water uptake capacity (Figure 18) compared to their counterparts having 1:1 ratio. In addition, cationic ions in CLN such as Ca^{2+}, Mg^{2+}, Na^{2+} provide strong water adsorption sites (Cakicioglu-Ozkan & Ulku, 2005). The presence of the CLN in the scaffolds caused no significant difference on the pore architecture compared to their counterparts without CLN (Figure 16).

4.3.2. Water Uptake and Weight Loss of CLN/PCEC Composite Scaffolds

Water absorption capacity of the scaffolds can offer capacity for proteins and other bodily solutes to be transported in and out of the scaffold and encourage cellular invasion (Long et al., 2015) welling study showed that pure PCEC and CLN/PCEC scaffolds can hold considerable amount of water within the structure. Consequently, the presence of the CLN in the scaffolds improved water adsorption (Figure 18).

CLN/PCEC scaffolds showed negligible degradation during two months in PBS under static conditions. Porosity of scaffolds did not have significant effect on the

hydrolytic degradation of scaffolds. PCEC copolymer in the scaffolds was synthesized by ring opening polymerization (ROP) where PCL and PEG units were bound together by covalent bonds via ester links in the backbone. As reported in the literature, PCL homopolymer and PCEC copolymer undergo hydrolytic cleavage in the polyester backbone and show an exponential weight loss over time (Eglin et al., 2009). In addition, it has been also stated that hydrolytic degradation can be accelerated in aggressive environments such as acidic or basic media for PCL-based scaffolds (E. K. Kim et al., 2014).

4.3.3. Mechanical Properties of CLN/PCEC Composite Scaffolds

CLN/PCEC scaffolds prepared using $NaHCO_3$ as porogen were analyzed for mechanical properties. In the stress-strain curves, the scaffolds with 1:2 (PCEC:$NaHCO_3$) ratio showed plateau region after 3% strain whereas continuous increase above 3% strain was observed for their 1:1 PCEC/$NaHCO_3$ counterparts (Figure 19A). The plateau region illustrates the collapse of the porous structure whereas the densification region represents the loss of mechanical support coming from the 3D structure (Hoyt et al., 2015). Therefore, 10% strain value was detected as the end of the plateau region where 3D architecture was completely destroyed. In our study, the failure under compression started at the end of linear elastic region close to 3% strain for all groups. Scaffolds in 1:2 group displayed elastomeric foam structure while 1:1 group displayed the elastic-plastic foam nature. All scaffold groups showed similar trends at the linear elastic region (Figure 19A). Initial increase in the modulus for both scaffold groups with 1:1 and 1:2 ratios might be explained as the outcome of the elasticity originating from copolymer matrix. However, overall porosity of groups might have caused weakness in the compressive strength of both groups. As indicated in literature, greater pore volume in structure leads to more stress concentration points around the peripheries of the pores (Rice, 1997). Therefore, lower porosity of scaffolds with 1:1 ratio provided significantly higher compressive properties compared to their counterparts with 1:2 ratio (Figure 19A and B). In addition, the presence of CLN in the scaffolds allowed resistance to higher compressive stresses compared to the scaffolds without CLN. Hence, the highest compressive moduli and ultimate strength

values were observed for scaffolds with the highest amount of CLN content and lowest porosity (Figure 19B).

4.3.4. Effect of CLN on Serum Protein Adsorption on CLN/PCEC Composite Scaffolds

CLN/PCEC scaffolds prepared using $NaHCO_3$ as porogen were analyzed for protein adsorption to determine the effect of CLN on protein adsorption capacity of scaffolds. Amount of weakly adsorbed serum proteins on the scaffold groups was found higher compared to the amount of strongly adsorbed proteins found on these groups. Weak protein adsorption on the CLN/PCEC composite and pure PCEC scaffolds could be related with the protein movement into pores of the scaffolds during incubation. On the other hand, robust electrostatic interactions between the proteins and scaffold surfaces lead to strong protein adsorption (Regis et al., 2014). Besides, it is reported that presence of a mineral content in the structure positively affects the protein adsorption process in scaffolds (Yangyang Li et al., 2014). For these reasons, CLN content in the scaffolds significantly increased the protein adsorption while pure PCEC scaffolds showed the lowest serum protein adsorption capacity (Figure 20A). Furthermore, enhanced serum protein adsorption on the scaffolds can create greater surface area where cell-adhesive ECM proteins are adsorbed and subsequently improves cellular attachment to the scaffolds (Woo et al., 2003). In a previous study, Kim et al. showed that scaffolds providing good serum protein adsorption increased cellular proliferation (H.-W. Kim et al., 2005). Consequently, higher protein adsorption on CLN containing scaffolds may lead to robust cellular attachment, proliferation and osteogenic differentiation.

4.3.5. Bioactivity of CLN/PCEC Composite Scaffolds

In all scaffold groups, CaP mineralization occurred in SBF solution (Figure 20B-G). Formation of CaP precipitation on scaffolds containing CLN occurred faster than the scaffolds without CLN (Figure 20B-G). CaP precipitation could be easily initiated with the interaction of phosphate ions from the SBF solution with the CLN due to the presence of positively charged calcium and magnesium ions in the periphery of the core silica-alumina framework of CLN. In accordance with the results of zeta potential

analysis of the CLN, the surface of the CLN was covered with OH^- ions. Hydroxyl ions are especially important in recruiting positively charged calcium ions to the surface and subsequently initiating CaP precipitation (Toworfe et al., 2006). Furthermore, silica in the backbone of the CLN is osteoinductive in terms of recruiting calcium ions reinforcing the phosphate ions for apatite nucleation (Aneta J Mieszawska et al., 2010). For 1:1+20% (PCEC:$NaHCO_3$+CLN%) scaffolds, initial Ca/P ratio in the first week (1.98) was found similar with the ratio of precursor CaP of biological apatite (Ocampo et al., 2015). Hence, HA deposition (Ca/P: 1.686) was observed on the scaffold containing highest amount of CLN (20%) (Figure 20G).

4.3.6. Evaluation of Cytocompatibility of CLN/PCEC Composite Scaffolds

In order to determine cytocompatibility of the scaffolds, hFOB cells were seeded onto CLN/PCEC composite and pure PCEC scaffolds. hFOB cells seeded on pure PCEC scaffolds showed higher cell viability compared to scaffolds containing CLN (1:1+10% and 1:1+20%) scaffolds at the end of first week (Figure 21A). This could be due to the higher porosity of pure PCEC scaffolds compared to other scaffolds (1:1+10% and 1:1+20%). However, there was a significant decrease in the cellular metabolic activity from 3rd day to 7th day (Figure 21A). This decrease can be explained by the osteogenic differentiation of hFOB cells in osteogenic medium (observed with ALP activity and intracellular calcium deposition at week 1, Figure 22A and B) which might have caused a decrease in cell proliferation. In addition, DNA quantification of hFOB cells on various scaffold groups showed an increase in cell number while CLN present groups showed significantly higher DNA content (Figure 21A). A similar finding was previously reported in the literature (Yongzhong Wang et al., 2005). Nonetheless, scaffolds containing CLN showed no cytotoxic effect on hFOB cells at all time points and significantly higher CaP mineral deposition by hFOB cells was observed at the end of 1st week (Figure 21B). ALP, an early osteogenic marker, is upregulated during osteogenic commitment (Lopez et al., 2005). ALP levels of hFOB cells seeded on scaffolds containing CLN (1:1+10% and 1:1+20%) peaked at the 1st week and displayed significantly higher value whereas ALP levels of cells on pure PCEC scaffold peaked at 3rd week (Figure 22A). Moreover, significantly higher OSP release, a late marker of osteogenic differentiation was also observed for the cells

seeded on the scaffolds containing CLN and OSP levels for these scaffolds peaked at the 3rd week (Figure 22B) (Holtorf et al., 2005). In agreement with ALP and OSP results, increased intracellular calcium depositions were found on hFOB cells seeded on 1:1+10% and 1:1+20% scaffolds (Figure 8C). Cells begin calcium intake prior to late stage of osteogenic differentiation (Katagiri & Takahashi, 2002). Then, calcium is released to form CaP deposits which will in return lead to nucleation of natural apatite and formation of bone ECM (Boonrungsiman et al., 2012). In agreement with the literature, ALP upregulation peaked as early as at the end of 1st week for the scaffolds containing CLN. Levels of OSP in the culture media increased gradually during the study in all groups while intracellular calcium content reached its maximum concentration at the end of 3rd week and quickly diminished after the initiation of osteogenic differentiation. It is also important to note that metallic activity of hFOB cells was lower at 2nd week for CLN containing scaffolds (1:1+10% and 1:1+20% scaffolds) compared to the pure PCEC scaffold (1:1 scaffold) while DNA quantity was higher for these scaffolds. In addition, higher levels of hFOB early differentiation markers such as ALP production and intracellular calcium deposition were observed in scaffolds containing CLN than those observed in pure PCEC scaffold at the end of first week. As pointed out by Rodrigues et al., cellular proliferation rate decreases significantly while cells differentiate (Rodrigues et al., 2012).

CHAPTER 5

CONCLUSION

This study presents reproducible solvent free powder compression/particulate leaching technique to produce scaffolds for BTE applications. It was shown that mineral, salt porogen and copolymer can be combined successfully without the use of organic solvents to produce highly interconnective, porous and mechanically strong composite scaffolds. Presence of CLN was shown to improve mechanical properties and in vitro protein adsorption capacity of the scaffolds. When the mineral content was 20% (w/w) of PCEC, compressive strength, compressive modulus and protein adsorption capacity of the scaffolds were immensely enhanced. In vitro bioactivity study demonstrated that increasing CLN content triggered faster CaP precipitation on the composite scaffolds. In vitro cell culture studies indicated that CLN presence promoted an osteoinductive environment for osteoblastic cells to proliferate and differentiate. The results collectively validate porous composite scaffolds containing bioactive and biocompatible mineral CLN hold promise to support bone tissue regeneration.

REFERENCES

Ahmad, M., Wahit, M. U., Abdul Kadir, M. R., & Mohd Dahlan, K. Z. (2012). Mechanical, rheological, and bioactivity properties of ultra high-molecular-weight polyethylene bioactive composites containing polyethylene glycol and hydroxyapatite. *The Scientific World Journal, 2012*.

Aho, J., Boetker, J. P., Baldursdottir, S., & Rantanen, J. (2015). Rheology as a tool for evaluation of melt processability of innovative dosage forms. *International Journal of Pharmaceutics, 494*(2), 623-642. doi: http://dx.doi.org/10.1016/j.ijpharm.2015.02.009

Akgül, M. S., N.B.; Özmak, M.; Dumanlı, A.G.; Yürüm, Y.; Karabakan, A. (2008). Adsorption of Bovine Serum Albumin (BSA) on Clinoptilolite. *Hacettepe Journal of Biology and Chemistry, 36*(1), 21-29.

Albrektsson, T., & Johansson, C. (2001). Osteoinduction, osteoconduction and osseointegration. *European Spine Journal, 10*(Suppl 2), S96-S101. doi: 10.1007/s005860100282

Amini, A. R., Laurencin, C. T., & Nukavarapu, S. P. (2012). Bone tissue engineering: recent advances and challenges. *Crit Rev Biomed Eng, 40*(5), 363-408.

Atila, D., Keskin, D., & Tezcaner, A. (2015). Cellulose acetate based 3-dimensional electrospun scaffolds for skin tissue engineering applications. *Carbohydrate Polymers, 133*, 251-261. doi: http://dx.doi.org/10.1016/j.carbpol.2015.06.109

Azhdar, B., Stenberg, B., & Kari, L. (2005). Development of a High-Velocity Compaction process for polymer powders. *Polymer Testing, 24*(7), 909-919. doi: http://dx.doi.org/10.1016/j.polymertesting.2005.06.008

Badylak, S. F., & Gilbert, T. W. (2008). Immune response to biologic scaffold materials. *Seminars in Immunology, 20*(2), 109-116. doi: http://dx.doi.org/10.1016/j.smim.2007.11.003

Barrère, F., van Blitterswijk, C. A., & de Groot, K. (2006). Bone regeneration: molecular and cellular interactions with calcium phosphate ceramics. *Int J Nanomedicine, 1*(3), 317-332.

Bedi, R. S., Beving, D. E., Zanello, L. P., & Yan, Y. (2009). Biocompatibility of corrosion-resistant zeolite coatings for titanium alloy biomedical implants. *Acta Biomater, 5*(8), 3265-3271. doi: http://dx.doi.org/10.1016/j.actbio.2009.04.019

Bhardwaj, N., & Kundu, S. C. (2010). Electrospinning: a fascinating fiber fabrication technique. *Biotechnol Adv, 28*(3), 325-347. doi: 10.1016/j.biotechadv.2010.01.004

Blanchard, S., & Bronzino, J. D. (2012). Chapter 3 - Anatomy and Physiology *Introduction to Biomedical Engineering (Third Edition)* (pp. 75-132). Boston: Academic Press.

Boonrungsiman, S., Gentleman, E., Carzaniga, R., Evans, N. D., McComb, D. W., Porter, A. E., & Stevens, M. M. (2012). The role of intracellular calcium phosphate in osteoblast-mediated bone apatite formation. *Proc Natl Acad Sci U S A, 109*(35), 14170-14175. doi: 10.1073/pnas.1208916109

Bose, S., Roy, M., & Bandyopadhyay, A. (2012). Recent advances in bone tissue engineering scaffolds. *Trends in Biotechnology, 30*(10), 546-554. doi: 10.1016/j.tibtech.2012.07.005

Bouropoulos, N., & Moradian–Oldak, J. (2003). Analysis of hydroxyapatite surface coverage by amelogenin nanospheres following the Langmuir model for protein adsorption. *Calcified tissue international, 72*(5), 599-603.

Brown, T. D., Dalton, P. D., & Hutmacher, D. W. (2011). Direct Writing By Way of Melt Electrospinning. *Advanced Materials, 23*(47), 5651-5657. doi: 10.1002/adma.201103482

Cakicioglu-Ozkan, F., & Ulku, S. (2005). The effect of HCl treatment on water vapor adsorption characteristics of clinoptilolite rich natural zeolite. *Microporous and Mesoporous Materials, 77*(1), 47-53. doi: http://dx.doi.org/10.1016/j.micromeso.2004.08.013

Callister, W. D., & William D., W. D. C. (2007). *Materials Science and Engineering: An Introduction, 7th Edition Wiley Plus Set*: John Wiley & Sons, Limited.

Capulli, M., Paone, R., & Rucci, N. (2014). Osteoblast and osteocyte: Games without frontiers. *Archives of Biochemistry and Biophysics, 561*, 3-12. doi: http://dx.doi.org/10.1016/j.abb.2014.05.003

Centola, M., Rainer, A., Spadaccio, C., Porcellinis, S. D., Genovese, J. A., & Trombetta, M. (2010). Combining electrospinning and fused deposition modeling for the fabrication of a hybrid vascular graft. *Biofabrication, 2*(1), 014102.

Chang, B.-S., Lee, C.-K., Hong, K.-S., Youn, H.-J., Ryu, H.-S., Chung, S.-S., & Park, K.-W. (2000). Osteoconduction at porous hydroxyapatite with various pore configurations. *Biomaterials, 21*(12), 1291-1298. doi: http://dx.doi.org/10.1016/S0142-9612(00)00030-2

Chang, K. Y., Cheng, L. W., Ho, G. H., Huang, Y. P., & Lee, Y. D. (2009). Fabrication and characterization of poly(gamma-glutamic acid)-graft-chondroitin sulfate/polycaprolactone porous scaffolds for cartilage tissue engineering. *Acta Biomater, 5*(6), 1937-1947. doi: 10.1016/j.actbio.2009.02.002

Chiku, H., Kawai, A., Ishibashi, T., Takehara, M., Yanai, T., Mizukami, F., & Sakaguchi, K. (2006). A novel protein refolding method using a zeolite. *Analytical biochemistry, 348*(2), 307-314.

Chong, E. J., Phan, T. T., Lim, I. J., Zhang, Y. Z., Bay, B. H., Ramakrishna, S., & Lim, C. T. (2007). Evaluation of electrospun PCL/gelatin nanofibrous scaffold for wound healing and layered dermal reconstitution. *Acta Biomater, 3*(3), 321-330. doi: http://dx.doi.org/10.1016/j.actbio.2007.01.002

Clarke, B. (2008). Normal Bone Anatomy and Physiology. *Clinical Journal of the American Society of Nephrology : CJASN, 3*(Suppl 3), S131-S139. doi: 10.2215/CJN.04151206

Clowes, J. A., Khosla, S., & Eastell, R. (2005). Potential role of pancreatic and enteric hormones in regulating bone turnover. *J Bone Miner Res, 20*(9), 1497-1506. doi: 10.1359/jbmr.050524

Cui, L., Zhang, N., Cui, W., Zhang, P., & Chen, X. (2015). A Novel Nano/Micro-Fibrous Scaffold by Melt-Spinning Method for Bone Tissue Engineering.

Journal of Bionic Engineering, 12(1), 117-128. doi: http://dx.doi.org/10.1016/S1672-6529(14)60106-2

Cundy, C. S., & Cox, P. A. (2003). The hydrothermal synthesis of zeolites: history and development from the earliest days to the present time. *Chemical reviews, 103*(3), 663-702. doi: 10.1021/cr020060i

Daculsi, G., Fellah, B. H., Miramond, T., & Durand, M. (2013). Osteoconduction, Osteogenicity, Osteoinduction, what are the fundamental properties for a smart bone substitutes. *IRBM, 34*(4–5), 346-348. doi: http://dx.doi.org/10.1016/j.irbm.2013.07.001

Dahlin, C., Johansson, A., Hoffman, M., & Molenberg, A. (2014). Early biocompatibility of poly (ethylene glycol) hydrogel barrier materials for guided bone regeneration. An in vitro study using human gingival fibroblasts (HGF-1). *Clinical Oral Implants Research, 25*(1), 16-20. doi: 10.1111/clr.12076

Dahlin, R. L., Kasper, F. K., & Mikos, A. G. (2011). Polymeric Nanofibers in Tissue Engineering. *Tissue Engineering Part B: Reviews, 17*(5), 349-364. doi: 10.1089/ten.teb.2011.0238

Dallas, S. L., Prideaux, M., & Bonewald, L. F. (2013). The Osteocyte: An Endocrine Cell … and More. *Endocrine Reviews, 34*(5), 658-690. doi: doi:10.1210/er.2012-1026

Dalton, P. D., Grafahrend, D., Klinkhammer, K., Klee, D., & Möller, M. (2007). Electrospinning of polymer melts: Phenomenological observations. *Polymer, 48*(23), 6823-6833. doi: http://dx.doi.org/10.1016/j.polymer.2007.09.037

Dalton, P. D., Vaquette, C., Farrugia, B. L., Dargaville, T. R., Brown, T. D., & Hutmacher, D. W. (2013). Electrospinning and additive manufacturing: converging technologies. *Biomaterials Science, 1*(2), 171-185. doi: 10.1039/C2BM00039C

Demirkiran, H., Mohandas, A., Dohi, M., Fuentes, A., Nguyen, K., & Aswath, P. (2010). Bioactivity and mineralization of hydroxyapatite with bioglass as sintering aid and bioceramics with Na3Ca6(PO4)5 and Ca5(PO4)2SiO4 in a silicate matrix. *Materials Science and Engineering: C, 30*(2), 263-272. doi: http://dx.doi.org/10.1016/j.msec.2009.10.011

Denhardt, D. T., & Guo, X. (1993). Osteopontin: a protein with diverse functions. *Faseb j, 7*(15), 1475-1482.

Dhamaniya, S., Das, D., Satapathy, B. K., & Jacob, J. (2012). Influence of block composition on structural, thermal and mechanical properties of novel aliphatic polyester based triblock copolymers. *Polymer, 53*(21), 4662-4671.

Dhandayuthapani, B. Y., Y.; Maekawa, T.; Kumar, D.S. (2011). Polymeric Scaffolds in Tissue Engineering Application: A Review. *International Journal of Polymer Science, 2011*. doi: 10.1155/2011/290602

Dimitriou, R., Jones, E., McGonagle, D., & Giannoudis, P. V. (2011). Bone regeneration: current concepts and future directions. *BMC Medicine, 9*(1), 1-10. doi: 10.1186/1741-7015-9-66

Dorozhkin, S. V. (2015). Calcium Orthophosphate-Containing Biocomposites and Hybrid Biomaterials for Biomedical Applications. *J Funct Biomater, 6*(3), 708-832. doi: 10.3390/jfb6030708

Du, Z. X., Xu, J. T., Yang, Y., & Fan, Z. Q. (2007). Synthesis and characterization of poly (ϵ-caprolactone)-b-poly (ethylene glycol) block copolymers prepared by a salicylaldimine-aluminum complex. *Journal of applied polymer science, 105*(2), 771-776.

Eglin, D., Mortisen, D., & Alini, M. (2009). Degradation of synthetic polymeric scaffolds for bone and cartilage tissue repairs. *Soft Matter, 5*(5), 938-947.

Erdemli, O., Captug, O., Bilgili, H., Orhan, D., Tezcaner, A., & Keskin, D. (2010). In vitro and in vivo evaluation of the effects of demineralized bone matrix or calcium sulfate addition to polycaprolactone-bioglass composites. *J Mater Sci Mater Med, 21*(1), 295-308. doi: 10.1007/s10856-009-3862-6

Erdemli, O., Keskin, D., & Tezcaner, A. (2015). Influence of excipients on characteristics and release profiles of poly(epsilon-caprolactone) microspheres containing immunoglobulin G. *Mater Sci Eng C Mater Biol Appl, 48*, 391-399. doi: 10.1016/j.msec.2014.12.044

Fan, M., Guo, Q., Luo, J., Luo, F., Xie, P., Tang, X., & Qian, Z. (2013). Preparation and in vitro characterization of dexamethasone-loaded poly(D,L-lactic acid) microspheres embedded in poly(ethylene glycol)-poly({varepsilon}-caprolactone)-poly(ethylene glycol) hydrogel for orthopedic tissue engineering. *J Biomater Appl, 28*(2), 288-297. doi: 10.1177/0885328212446097

Fatouros, D. G., Douroumis, D., Nikolakis, V., Ntais, S., Moschovi, A., Trivedi, V., . . . Cox, P. A. (2011). In vitro and in silico investigations of drug delivery via zeolite BEA. *Journal of Materials Chemistry, 21*(21). doi: 10.1039/c1jm10204d

Feng, R., Song, Z., & Zhai, G. (2012). Preparation and in vivo pharmacokinetics of curcumin-loaded PCL-PEG-PCL triblock copolymeric nanoparticles. *Int J Nanomedicine, 7*, 4089-4098. doi: 10.2147/ijn.s33607

Florencio-Silva, R., Sasso, G. R. d. S., Sasso-Cerri, E., Sim, #xf5, es, M. J., . . . rgio. (2015). Biology of Bone Tissue: Structure, Function, and Factors That Influence Bone Cells. *BioMed Research International, 2015*, 17. doi: 10.1155/2015/421746

Fong, E. L., Chan, C. K., & Goodman, S. B. (2011). Stem cell homing in musculoskeletal injury. *Biomaterials, 32*(2), 395-409. doi: 10.1016/j.biomaterials.2010.08.101

Fu, S., Yang, L., Fan, J., Wen, Q., Lin, S., Wang, B., . . . Wu, J. (2013). In vitro mineralization of hydroxyapatite on electrospun poly(ε-caprolactone)–poly(ethylene glycol)–poly(ε-caprolactone) fibrous scaffolds for tissue engineering application. *Colloids and Surfaces B: Biointerfaces, 107*, 167-173. doi: http://dx.doi.org/10.1016/j.colsurfb.2013.01.068

Gautam, S., Dinda, A. K., & Mishra, N. C. (2013). Fabrication and characterization of PCL/gelatin composite nanofibrous scaffold for tissue engineering applications by electrospinning method. *Materials Science and Engineering: C, 33*(3), 1228-1235. doi: http://dx.doi.org/10.1016/j.msec.2012.12.015

Gentile, P., Mattioli-Belmonte, M., Chiono, V., Ferretti, C., Baino, F., Tonda-Turo, C., . . . Ciardelli, G. (2012). Bioactive glass/polymer composite scaffolds

mimicking bone tissue. *Journal of Biomedical Materials Research Part A, 100*(10), 2654-2667.

Geris, L., Vander Sloten, J., & Van Oosterwyck, H. (2009). In silico biology of bone modelling and remodelling: regeneration. *Philosophical Transactions of the Royal Society of London A: Mathematical, Physical and Engineering Sciences, 367*(1895), 2031-2053. doi: 10.1098/rsta.2008.0293

Glimcher, M. J. (1987). The nature of the mineral component of bone and the mechanism of calcification. *Instr Course Lect, 36*, 49-69.

Gloria, A., De Santis, R., & Ambrosio, L. (2010). Polymer-based composite scaffolds for tissue engineering. *J Appl Biomater Biomech, 8*(2), 57-67.

Gómez-Barrena, E., Rosset, P., Lozano, D., Stanovici, J., Ermthaller, C., & Gerbhard, F. (2015). Bone fracture healing: Cell therapy in delayed unions and nonunions. *Bone, 70*, 93-101. doi: http://dx.doi.org/10.1016/j.bone.2014.07.033

Gong, C., Qian, Z., Liu, C., Huang, M., Gu, Y., Wen, Y., . . . Li, X. (2007). A thermosensitive hydrogel based on biodegradable amphiphilic poly (ethylene glycol)–polycaprolactone–poly (ethylene glycol) block copolymers*Smart materials and structures, 16*(3), 927.

Gürbüz, S., Demirtaş, T. T., Yüksel, E., Karakeçili, A., Doğan, A., & Gümüşderelioğlu, M. (2016). Multi-layered functional membranes for periodontal regeneration: Preparation and characterization. *Materials Letters, 178*, 256-259. doi: http://dx.doi.org/10.1016/j.matlet.2016.05.054

Hadjidakis, D. J., & Androulakis, I. I. (2006). Bone Remodeling. *Annals of the New York Academy of Sciences, 1092*(1), 385-396. doi: 10.1196/annals.1365.035

Harvey, E. J., Henderson, J. E., & Vengallatore, S. T. (2010). Nanotechnology and bone healing. *J Orthop Trauma, 24 Suppl 1*, S25-30. doi: 10.1097/BOT.0b013e3181ca3b58

Haugen, H., Ried, V., Brunner, M., Will, J., & Wintermantel, E. (2004). Water as foaming agent for open cell polyurethane structures. *Journal of Materials Science: Materials in Medicine, 15*(4), 343-346. doi: 10.1023/B:JMSM.0000021099.33619.ac

Hauschka, P. V. (1986). Osteocalcin: the vitamin K-dependent Ca2+-binding protein of bone matrix. *Haemostasis, 16*(3-4), 258-272.

Hemmati, K., Alizadeh, R., & Ghaemy, M. (2015). Synthesis and characterization of controlled drug release carriers based on functionalized amphiphilic block copolymers and super-paramagnetic iron oxide nanoparticles. *Polymers for Advanced Technologies*.

Hench, L. L., & Polak, J. M. (2002). Third-Generation Biomedical Materials. *Science, 295*(5557), 1014-1017. doi: 10.1126/science.1067404

Henkel, J., Woodruff, M. A., Epari, D. R., Steck, R., Glatt, V., Dickinson, I. C., . . . Hutmacher, D. W. (2013). Bone Regeneration Based on Tissue Engineering Conceptions — A 21st Century Perspective. *Bone Research, 1*, 216. doi: 10.4248/BR201303002

Heo, S. J., Kim, S. E., Wei, J., Hyun, Y. T., Yun, H. S., Kim, D. H., . . . Shin, J. W. (2009). Fabrication and characterization of novel nano- and micro-HA/PCL

composite scaffolds using a modified rapid prototyping process. *J Biomed Mater Res A, 89*(1), 108-116. doi: 10.1002/jbm.a.31726

Hollinger, J. O., Einhorn, T. A., Doll, B., & Sfeir, C. (2004). *Bone Tissue Engineering*: Taylor & Francis.

Holtorf, H. L., Datta, N., Jansen, J. A., & Mikos, A. G. (2005). Scaffold mesh size affects the osteoblastic differentiation of seeded marrow stromal cells cultured in a flow perfusion bioreactor. *Journal of Biomedical Materials Research Part A, 74*(2), 171-180.

Hoque, M. E., San, W. Y., Wei, F., Li, S., Huang, M. H., Vert, M., & Hutmacher, D. W. (2009). Processing of polycaprolactone and polycaprolactone-based copolymers into 3D scaffolds, and their cellular responses. *Tissue Eng Part A, 15*(10), 3013-3024. doi: 10.1089/ten.TEA.2008.0355

Hoyt, A. J., Yakacki, C. M., Fertig, R. S., 3rd, Dana Carpenter, R., & Frick, C. P. (2015). Monotonic and cyclic loading behavior of porous scaffolds made from poly(para-phenylene) for orthopedic applications. *J Mech Behav Biomed Mater, 41*, 136-148. doi: 10.1016/j.jmbbm.2014.10.004

Huang, G. X., Arany, P. R., & Mooney, D. J. (2015). Modeling and Validation of Multilayer Poly(Lactide-Co-Glycolide) Scaffolds for In Vitro Directed Differentiation of Juxtaposed Cartilage and Bone. *Tissue Engineering Part A, 21*(15-16), 2228-2240. doi: 10.1089/ten.tea.2015.0089

Huang, M.-H., Li, S., Coudane, J., & Vert, M. (2003). Synthesis and Characterization of Block Copolymers of ε-Caprolactone and DL-Lactide Initiated by Ethylene Glycol or Poly(ethylene glycol). *Macromolecular Chemistry and Physics, 204*(16), 1994-2001. doi: 10.1002/macp.200350054

Huang, M. H., Li, S., Hutmacher, D. W., Schantz, J. T., Vacanti, C. A., Braud, C., & Vert, M. (2004). Degradation and cell culture studies on block copolymers prepared by ring opening polymerization of epsilon-caprolactone in the presence of poly(ethylene glycol). *J Biomed Mater Res A, 69*(3), 417-427. doi: 10.1002/jbm.a.30008

Kane, R. J., Weiss-Bilka, H. E., Meagher, M. J., Liu, Y., Gargac, J. A., Niebur, G. L., . . . Roeder, R. K. (2015). Hydroxyapatite reinforced collagen scaffolds with improved architecture and mechanical properties. *Acta Biomater, 17*, 16-25. doi: 10.1016/j.actbio.2015.01.031

Karageorgiou, V., & Kaplan, D. (2005). Porosity of 3D biomaterial scaffolds and osteogenesis. *Biomaterials, 26*(27), 5474-5491. doi: 10.1016/j.biomaterials.2005.02.002

Katagiri, T., & Takahashi, N. (2002). Regulatory mechanisms of osteoblast and osteoclast differentiation. *Oral Diseases, 8*(3), 147-159. doi: 10.1034/j.1601-0825.2002.01829.x

Keating, J. F., Simpson, A. H. R. W., & Robinson, C. M. (2005). The management of fractures with bone loss. *Bone & Joint Journal, 87-B*(2), 142-150. doi: 10.1302/0301-620x.87b2.15874

Kim, E. K., Pant, H. R., Hwang, B. S., Kim, Y. K., Kim, H. Y., Lee, K. M., . . . Kim, C. S. (2014). Influence of lactic acid on degradation and biocompatibility of electrospun poly (ε-caprolactone) fibers. *Polymer International, 63*(7), 1212-1218.

Kim, H.-W., Kim, H.-E., & Salih, V. (2005). Stimulation of osteoblast responses to biomimetic nanocomposites of gelatin–hydroxyapatite for tissue engineering scaffolds. *Biomaterials, 26*(25), 5221-5230.

Kim, Y. B., & Kim, G. H. (2015). PCL/Alginate Composite Scaffolds for Hard Tissue Engineering: Fabrication, Characterization, and Cellular Activities. *ACS Combinatorial Science, 17*(2), 87-99. doi: 10.1021/co500033h

Kinard, L. A., Chu, C.-Y., Tabata, Y., Kasper, K. F., & Mikos, A. G. (2013). Bone Morphogenetic Protein-2 Release from Composite Hydrogels of Oligo(poly(ethylene glycol) fumarate) and Gelatin. *Pharmaceutical Research, 30*(9), 2332-2343. doi: 10.1007/s11095-013-1077-5

Kindblom, J. M., Ohlsson, C., Ljunggren, O., Karlsson, M. K., Tivesten, A., Smith, U., & Mellstrom, D. (2009). Plasma osteocalcin is inversely related to fat mass and plasma glucose in elderly Swedish men. *J Bone Miner Res, 24*(5), 785-791. doi: 10.1359/jbmr.081234

Kirdeciler, S. K., Ozen, C., & Akata, B. (2014). Fabrication of nano-to micron-sized patterns using zeolites: Its application in BSA adsorption. *Microporous and Mesoporous Materials, 191*, 59-66.

Knop, K., Hoogenboom, R., Fischer, D., & Schubert, U. S. (2010). Poly(ethylene glycol) in drug delivery: pros and cons as well as potential alternatives. *Angew Chem Int Ed Engl, 49*(36), 6288-6308. doi: 10.1002/anie.200902672

Kohane, D. S., & Langer, R. (2008). Polymeric Biomaterials in Tissue Engineering. *Pediatr Res, 63*(5), 487-491.

Kokubo, T., & Takadama, H. (2006). How useful is SBF in predicting in vivo bone bioactivity? *Biomaterials, 27*(15), 2907-2915. doi: 10.1016/j.biomaterials.2006.01.017

Kothapalli, C. R., Wei, M., & Shaw, M. T. (2008). Solvent-specific gel-like transition via complexation of polyelectrolyte and hydroxyapatite nanoparticles suspended in water-glycerin mixtures: a rheological study. *Soft Matter, 4*(3), 600-605. doi: 10.1039/B713331F

Krohn, J. E., & Tsapatsis, M. (2005). Amino acid adsorption on zeolite β. *Langmuir, 21*(19), 8743-8750.

Kutikov, A. B., & Song, J. (2013). An amphiphilic degradable polymer/hydroxyapatite composite with enhanced handling characteristics promotes osteogenic gene expression in bone marrow stromal cells. *Acta Biomaterialia, 9*(9), 8354-8364. doi: http://dx.doi.org/10.1016/j.actbio.2013.06.013

Lasanianos, N. G., Kanakaris, N. K., & Giannoudis, P. V. (2010). Current management of long bone large segmental defects. *Orthopaedics and Trauma, 24*(2), 149-163. doi: 10.1016/j.mporth.2009.10.003

LeGeros, R. Z., Lin, S., Rohanizadeh, R., Mijares, D., & LeGeros, J. P. (2003). Biphasic calcium phosphate bioceramics: preparation, properties and applications. *Journal of Materials Science: Materials in Medicine, 14*(3), 201-209. doi: 10.1023/a:1022872421333

Leong, K. F., Cheah, C. M., & Chua, C. K. (2003). Solid freeform fabrication of three-dimensional scaffolds for engineering replacement tissues and organs.

Biomaterials, 24(13), 2363-2378. doi: http://dx.doi.org/10.1016/S0142-9612(03)00030-9

Li, H., & Chang, J. (2013). Bioactive silicate materials stimulate angiogenesis in fibroblast and endothelial cell co-culture system through paracrine effect. *Acta Biomater, 9*(6), 6981-6991. doi: http://dx.doi.org/10.1016/j.actbio.2013.02.014

Li, Y., Chen, S.-K., Li, L., Qin, L., Wang, X.-L., & Lai, Y.-X. (2015). Bone defect animal models for testing efficacy of bone substitute biomaterials. *Journal of Orthopaedic Translation, 3*(3), 95-104. doi: http://dx.doi.org/10.1016/j.jot.2015.05.002

Li, Y., Li, B., Xu, G., Ahmad, Z., Ren, Z., Dong, Y., . . . Han, G. (2014). A feasible approach toward bioactive glass nanofibers with tunable protein release kinetics for bone scaffolds. *Colloids and Surfaces B: Biointerfaces, 122*, 785-791.

Li, Y., Liao, X., Zhang, X., Ma, G., Zuo, S., Xiao, L., . . . Fan, J. (2014). In situ generated thrombin in the protein corona of zeolites: Relevance of the functional proteins to its biological impact. *Nano Research, 7*(10), 1457-1465. doi: 10.1007/s12274-014-0505-0

Liang, C., Joseph, M. M., James, C. M. L., & Hao, L. (2011). The role of surface charge on the uptake and biocompatibility of hydroxyapatite nanoparticles with osteoblast cells. *Nanotechnology, 22*(10), 105708.

Liao, C.-J., Chen, C.-F., Chen, J.-H., Chiang, S.-F., Lin, Y.-J., & Chang, K.-Y. (2002). Fabrication of porous biodegradable polymer scaffolds using a solvent merging/particulate leaching method. *J Biomed Mater Res, 59*(4), 676-681. doi: 10.1002/jbm.10030

Lim, Y.-M., Gwon, H.-J., Shin, J., Jeun, J. P., & Nho, Y. C. (2008). Preparation of porous poly(ε-caprolactone) scaffolds by gas foaming process and in vitro/in vivo degradation behavior using γ-ray irradiation. *Journal of Industrial and Engineering Chemistry, 14*(4), 436-441. doi: http://dx.doi.org/10.1016/j.jiec.2008.01.019

Lin, Z., Cao, S., Chen, X., Wu, W., & Li, J. (2013). Thermoresponsive hydrogels from phosphorylated ABA triblock copolymers: a potential scaffold for bone tissue engineering. *Biomacromolecules, 14*(7), 2206-2214. doi: 10.1021/bm4003442

Liu, C. B., Gong, C. Y., Huang, M. J., Wang, J. W., Pan, Y. F., Zhang, Y. D., . . . Qian, Z. Y. (2008). Thermoreversible gel–sol behavior of biodegradable PCL-PEG-PCL triblock copolymer in aqueous solutions. *Journal of Biomedical Materials Research Part B: Applied Biomaterials, 84B*(1), 165-175. doi: 10.1002/jbm.b.30858

Liu, Y., Lim, J., & Teoh, S. H. (2013). Review: development of clinically relevant scaffolds for vascularised bone tissue engineering. *Biotechnol Adv, 31*(5), 688-705. doi: 10.1016/j.biotechadv.2012.10.003

Lo Re, G., Lopresti, F., Petrucci, G., & Scaffaro, R. (2015). A facile method to determine pore size distribution in porous scaffold by using image processing. *Micron, 76*, 37-45. doi: http://dx.doi.org/10.1016/j.micron.2015.05.001

Logeart-Avramoglou, D., Anagnostou, F., Bizios, R., & Petite, H. (2005). Engineering bone: challenges and obstacles. *J Cell Mol Med, 9*(1), 72-84.

Long, T., Yang, J., Shi, S. S., Guo, Y. P., Ke, Q. F., & Zhu, Z. A. (2015). Fabrication of three-dimensional porous scaffold based on collagen fiber and bioglass for bone tissue engineering. *Journal of Biomedical Materials Research Part B: Applied Biomaterials, 103*(7), 1455-1464.

Lopez, V. C., Hadgraft, J., & Snowden, M. J. (2005). The use of colloidal microgels as a (trans)dermal drug delivery system. *Int J Pharm, 292*(1-2), 137-147. doi: 10.1016/j.ijpharm.2004.11.040

Ma, G., Miao, B., & Song, C. (2010). Thermosensitive PCL-PEG-PCL hydrogels: Synthesis, characterization, and delivery of proteins. *Journal of applied polymer science, 116*(4), 1985-1993.

Machado do Reis, L., Kessler, C. B., Adams, D. J., Lorenzo, J., Jorgetti, V., & Delany, A. M. (2008). Accentuated osteoclastic response to parathyroid hormone undermines bone mass acquisition in osteonectin-null mice. *Bone, 43*(2), 264-273. doi: http://dx.doi.org/10.1016/j.bone.2008.03.024

Maier, J. A. M., Bernardini, D., Rayssiguier, Y., & Mazur, A. (2004). High concentrations of magnesium modulate vascular endothelial cell behaviour in vitro. *Biochimica et Biophysica Acta (BBA) - Molecular Basis of Disease, 1689*(1), 6-12. doi: http://dx.doi.org/10.1016/j.bbadis.2004.02.004

Makadia, H. K., & Siegel, S. J. (2011). Poly Lactic-co-Glycolic Acid (PLGA) as Biodegradable Controlled Drug Delivery Carrier. *Polymers, 3*(3), 1377-1397. doi: 10.3390/polym3031377

Malaval, L., Wade-Guéye, N. M., Boudiffa, M., Fei, J., Zirngibl, R., Chen, F., . . . Aubin, J. E. (2008). Bone sialoprotein plays a functional role in bone formation and osteoclastogenesis. *The Journal of Experimental Medicine, 205*(5), 1145-1153. doi: 10.1084/jem.20071294

Mathieu, L. M., Bourban, P. E., & Månson, J. A. E. (2006). Processing of homogeneous ceramic/polymer blends for bioresorbable composites. *Composites Science and Technology,66*(11–12),1606-1614.doi: http://dx.doi.org/10.1016/j.compscitech.2005.11.012

Mazhuga, P. M. (1984). Mechanisms of cartilage precursor replacement by bone in the mammalian skeleton. *Acta Biol Hung, 35*(2-4), 219-225.

Mieszawska, A. J., Fourligas, N., Georgakoudi, I., Ouhib, N. M., Belton, D. J., Perry, C. C., & Kaplan, D. L. (2010). Osteoinductive silk–silica composite biomaterials for bone regeneration. *Biomaterials, 31*(34), 8902-8910.

Mieszawska, A. J., Llamas, J. G., Vaiana, C. A., Kadakia, M. P., Naik, R. R., & Kaplan, D. L. (2011). Clay enriched silk biomaterials for bone formation. *Acta Biomater, 7*(8), 3036-3041. doi: http://dx.doi.org/10.1016/j.actbio.2011.04.016

Moon, H. T., Lee, Y.-K., Han, J. K., & Byun, Y. (2002). Improved blood compatibility by sustained release of heparin–deoxycholic acid conjugates in a PCL–PEG multiblock copolymer matrix. *Journal of Biomaterials Science, Polymer Edition, 13*(7), 817-828. doi: 10.1163/156856202760197438

Moroni, L., de Wijn, J. R., & van Blitterswijk, C. A. (2008). Integrating novel technologies to fabricate smart scaffolds. *Journal of Biomaterials Science, Polymer Edition, 19*(5), 543-572. doi: 10.1163/156856208784089571

Morrison, S. J., & Scadden, D. T. (2014). The bone marrow niche for haematopoietic stem cells. *Nature, 505*(7483), 327-334. doi: 10.1038/nature12984

Mouriño, V., & Boccaccini, A. R. (2010). Bone tissue engineering therapeutics: controlled drug delivery in three-dimensional scaffolds. *Journal of The Royal Society Interface, 7*(43), 209-227. doi: 10.1098/rsif.2009.0379

Müller, K. H., Motskin, M., Philpott, A. J., Routh, A. F., Shanahan, C. M., Duer, M. J., & Skepper, J. N. (2014). The effect of particle agglomeration on the formation of a surface-connected compartment induced by hydroxyapatite nanoparticles in human monocyte-derived macrophages. *Biomaterials, 35*(3), 1074-1088. doi: http://dx.doi.org/10.1016/j.biomaterials.2013.10.041

Nair, L. S., & Laurencin, C. T. (2007). Biodegradable polymers as biomaterials. *Progress in Polymer Science, 32*(8–9), 762-798. doi: http://dx.doi.org/10.1016/j.progpolymsci.2007.05.017

Naumenko, E. A., Guryanov, I. D., Yendluri, R., Lvov, Y. M., & Fakhrullin, R. F. (2016). Clay nanotube-biopolymer composite scaffolds for tissue engineering. *Nanoscale, 8*(13), 7257-7271. doi: 10.1039/C6NR00641H

Nicolais, L., Gloria, A., & Ambrosio, L. (2010). 17 - The mechanics of biocomposites *Biomedical Composites* (pp. 411-440): Woodhead Publishing.

Ninan, N., Grohens, Y., Elain, A., Kalarikkal, N., & Thomas, S. (2013). Synthesis and characterisation of gelatin/zeolite porous scaffold. *European Polymer Journal, 49*(9). doi: 10.1016/j.eurpolymj.2013.02.014

Niu, Y., Dong, W., Guo, H., Deng, Y., Guo, L., An, X., . . . Li, M. (2014). Mesoporous magnesium silicate-incorporated poly(epsilon-caprolactone)-poly(ethylene glycol)-poly(epsilon-caprolactone) bioactive composite beneficial to osteoblast behaviors. *Int J Nanomedicine, 9*, 2665-2675. doi: 10.2147/ijn.s59040

Nuttelman, C. R., Tripodi, M. C., & Anseth, K. S. (2005). Synthetic hydrogel niches that promote hMSC viability. *Matrix Biol, 24*(3), 208-218. doi: 10.1016/j.matbio.2005.03.004

Ocampo, J. I. G., Sierra, D. M. E., & Orozco, C. P. O. (2015). Porous bodies of hydroxyapatite produced by a combination of the gel-casting and polymer sponge methods. *Journal of Advanced Research*.

Olad, A., & Farshi Azhar, F. (2014). The synergetic effect of bioactive ceramic and nanoclay on the properties of chitosan–gelatin/nanohydroxyapatite–montmorillonite scaffold for bone tissue engineering. *Ceramics International, 40*(7, Part A), 10061-10072. doi: http://dx.doi.org/10.1016/j.ceramint.2014.04.010

Orimo, H. (2010). The Mechanism of Mineralization and the Role of Alkaline Phosphatase in Health and Disease. *Journal of Nippon Medical School, 77*(1), 4-12. doi: 10.1272/jnms.77.4

Oryan, A., Alidadi, S., Moshiri, A., & Maffulli, N. (2014). Bone regenerative medicine: classic options, novel strategies, and future directions. *Journal of Orthopaedic Surgery and Research, 9*, 18-18. doi: 10.1186/1749-799X-9-18

Ozcelik, B., Blencowe, A., Palmer, J., Ladewig, K., Stevens, G. W., Abberton, K. M., . . . Qiao, G. G. (2014). Highly porous and mechanically robust polyester

poly(ethylene glycol) sponges as implantable scaffolds. *Acta Biomaterialia, 10*(6), 2769-2780. doi: http://dx.doi.org/10.1016/j.actbio.2014.02.019

Park, H. J., Lee, O. J., Lee, M. C., Moon, B. M., Ju, H. W., min Lee, J., . . . Park, C. H. (2015). Fabrication of 3D porous silk scaffolds by particulate (salt/sucrose) leaching for bone tissue reconstruction. *International journal of biological macromolecules, 78*, 215-223.

Pereira, T., Silva, M., Oliveira, M., Maia, I., Silva, J., Costa, M., & Thiré, R. (2012). Effect of process parameters on the properties of selective laser sintered Poly (3-hydroxybutyrate) scaffolds for bone tissue engineering. *Virtual and Physical Prototyping, 7*(4), 275-285.

Pietak, A. M., Reid, J. W., Stott, M. J., & Sayer, M. (2007). Silicon substitution in the calcium phosphate bioceramics. *Biomaterials, 28*(28), 4023-4032. doi: http://dx.doi.org/10.1016/j.biomaterials.2007.05.003

Poologasundarampillai, G., Wang, D., Li, S., Nakamura, J., Bradley, R., Lee, P. D., . . . Jones, J. R. (2014). Cotton-wool-like bioactive glasses for bone regeneration. *Acta Biomater, 10*(8), 3733-3746. doi: http://dx.doi.org/10.1016/j.actbio.2014.05.020

Puppi, D., Chiellini, F., Piras, A. M., & Chiellini, E. (2010). Polymeric materials for bone and cartilage repair. *Progress in Polymer Science, 35*(4). doi: 10.1016/j.progpolymsci.2010.01.006

Reddi, A. H., Gay, R., Gay, S., & Miller, E. J. (1977). Transitions in collagen types during matrix-induced cartilage, bone, and bone marrow formation. *Proceedings of the National Academy of Sciences, 74*(12), 5589-5592.

Regis, S., Youssefian, S., Jassal, M., Phaneuf, M. D., Rahbar, N., & Bhowmick, S. (2014). Fibronectin adsorption on functionalized electrospun polycaprolactone scaffolds: Experimental and molecular dynamics studies. *Journal of Biomedical Materials Research Part A, 102*(6), 1697-1706.

Rezwan, K., Chen, Q. Z., Blaker, J. J., & Boccaccini, A. R. (2006). Biodegradable and bioactive porous polymer/inorganic composite scaffolds for bone tissue engineering. *Biomaterials, 27*(18), 3413-3431. doi: http://dx.doi.org/10.1016/j.biomaterials.2006.01.039

Rhee, S.-H., Lee, J. D., & Tanaka, J. (2000). Nucleation of Hydroxyapatite Crystal through Chemical Interaction with Collagen. *Journal of the American Ceramic Society, 83*(11), 2890-2892. doi: 10.1111/j.1151-2916.2000.tb01656.x

Rho, J.-Y., Kuhn-Spearing, L., & Zioupos, P. Mechanical properties and the hierarchical structure of bone. *Medical Engineering and Physics, 20*(2), 92-102. doi: 10.1016/S1350-4533(98)00007-1

Rice, R. W. (1997). Limitations of pore-stress concentrations on the mechanical properties of porous materials. *Journal of Materials Science, 32*(17), 4731-4736. doi: 10.1023/a:1018674713006

Rodrigues, M. T., Lee, B. K., Lee, S. J., Gomes, M. E., Reis, R. L., Atala, A., & Yoo, J. J. (2012). The effect of differentiation stage of amniotic fluid stem cells on bone regeneration. *Biomaterials, 33*(26), 6069-6078. doi: 10.1016/j.biomaterials.2012.05.016

Rosen, C. J. (2008). Bone remodeling, energy metabolism, and the molecular clock. *Cell Metab, 7*(1), 7-10. doi: 10.1016/j.cmet.2007.12.004

Roy, T. D., Simon, J. L., Ricci, J. L., Rekow, E. D., Thompson, V. P., & Parsons, J. R. (2003). Performance of degradable composite bone repair products made via three-dimensional fabrication techniques. *Journal of Biomedical Materials Research Part A, 66*(2), 283-291.

Sabir, M. I., Xu, X., & Li, L. (2009). A review on biodegradable polymeric materials for bone tissue engineering applications. *Journal of Materials Science, 44*(21), 5713-5724. doi: 10.1007/s10853-009-3770-7

Saidak, Z., & Marie, P. J. (2012). Strontium signaling: Molecular mechanisms and therapeutic implications in osteoporosis. *Pharmacology & Therapeutics, 136*(2), 216-226. doi: http://dx.doi.org/10.1016/j.pharmthera.2012.07.009

Sainz, M. A., Pena, P., Serena, S., & Caballero, A. (2010). Influence of design on bioactivity of novel CaSiO3–CaMg(SiO3)2 bioceramics: In vitro simulated body fluid test and thermodynamic simulation. *Acta Biomater, 6*(7), 2797-2807. doi: http://dx.doi.org/10.1016/j.actbio.2010.01.003

Scaffaro, R., Lopresti, F., Botta, L., Rigogliuso, S., & Ghersi, G. (2016). Preparation of three-layered porous PLA/PEG scaffold: relationship between morphology, mechanical behavior and cell permeability. *J Mech Behav Biomed Mater, 54*, 8-20. doi: http://dx.doi.org/10.1016/j.jmbbm.2015.08.033

Schainberg, A. P. M., Özyeğin, L., Kursuoğlu, P., Valério, P., Goes, A., & Leite, F. M. (2005). Biocompatibility Evaluation of Zeolite Compared to Bone HA, Calcium Phosphate (Ca_2PO_4) and Eugenol Paste. *Key Engineering Materials, 284-286*, 561564. doi: 10.4028/www.scientific.net/KEM.284-286.561

Seifu, D. G., Isimjan, T. T., & Mequanint, K. (2011). Tissue engineering scaffolds containing embedded fluorinated-zeolite oxygen vectors. *Acta Biomater, 7*(10), 3670-3678. doi: 10.1016/j.actbio.2011.06.010

Serra, T., Ortiz-Hernandez, M., Engel, E., Planell, J. A., & Navarro, M. (2014). Relevance of PEG in PLA-based blends for tissue engineering 3D-printed scaffolds. *Materials Science and Engineering: C, 38*, 55-62. doi: 10.1016/j.msec.2014.01.003

Setzer, B., Bachle, M., Metzger, M. C., & Kohal, R. J. (2009). The gene-expression and phenotypic response of hFOB 1.19 osteoblasts to surface-modified titanium and zirconia. *Biomaterials, 30*(6), 979-990. doi: 10.1016/j.biomaterials.2008.10.054

Shea, L. D., Wang, D., Franceschi, R. T., & Mooney, D. J. (2000). Engineered bone development from a pre-osteoblast cell line on three-dimensional scaffolds. *Tissue Eng, 6*(6), 605-617. doi: 10.1089/10763270050199550

Shi, Q., Zhou, Y., & Sun, Y. (2005). Influence of pH and Ionic Strength on the Steric Mass-Action Model Parameters around the Isoelectric Point of Protein. *Biotechnology progress, 21*(2), 516-523.

Shrivats, A. R., McDermott, M. C., & Hollinger, J. O. (2014). Bone tissue engineering: state of the union. *Drug Discov Today, 19*(6), 781-786. doi: 10.1016/j.drudis.2014.04.010

Siddiq, A. R., & Kennedy, A. R. (2015). Porous poly-ether ether ketone (PEEK) manufactured by a novel powder route using near-spherical salt bead porogens: Characterisation and mechanical properties. *Materials Science and*

Engineering: C, 47, 180-188. doi: http://dx.doi.org/10.1016/j.msec.2014.11.044

Smith, L. A., Liu, X., Hu, J., & Ma, P. X. (2010). The enhancement of human embryonic stem cell osteogenic differentiation with nano-fibrous scaffolding. *Biomaterials, 31*(21), 5526-5535. doi: 10.1016/j.biomaterials.2010.03.065

Sosnik, A., & Cohn, D. (2003). Poly(ethylene glycol)-poly(epsilon-caprolactone) block oligomers as injectable materials. *Polymer*, *44*(23), 70337042. doi: 10.1016/j.polymer.2003.09.012

Stevens, B., Yang, Y., Mohandas, A., Stucker, B., & Nguyen, K. T. (2008). A review of materials, fabrication methods, and strategies used to enhance bone regeneration in engineered bone tissues. *Journal of Biomedical Materials Research Part B: Applied Biomaterials, 85B*(2), 573-582. doi: 10.1002/jbm.b.30962

Szarpak-Jankowska, A., Burgess, C., De Cola, L., & Huskens, J. (2013). Cyclodextrin-Modified Zeolites: Host–Guest Surface Chemistry for the Construction of Multifunctional Nanocontainers. *Chemistry – A European Journal, 19*(44), 14925-14930. doi: 10.1002/chem.201302153

Taqvi, S., & Roy, K. (2006). Influence of scaffold physical properties and stromal cell coculture on hematopoietic differentiation of mouse embryonic stem cells. *Biomaterials, 27*(36), 6024-6031. doi: 10.1016/j.biomaterials.2006.05.052

Tavolaro, A., Tavolaro, P., & Drioli, E. (2007). Zeolite inorganic supports for BSA immobilization: Comparative study of several zeolite crystals and composite membranes. *Colloids and Surfaces B: Biointerfaces, 55*(1), 67-76.

Thadavirul, N., Pavasant, P., & Supaphol, P. (2014). Development of polycaprolactone porous scaffolds by combining solvent casting, particulate leaching, and polymer leaching techniques for bone tissue engineering. *J Biomed Mater Res A, 102*(10), 3379-3392. doi: 10.1002/jbma.35010

Thomson, R. C., Wake, M. C., Yaszemski, M. J., & Mikos, A. G. (1995). Biodegradable polymer scaffolds to regenerate organs. In N. A. Peppas & R. S. Langer (Eds.), *Biopolymers II* (pp. 245-274). Berlin, Heidelberg: Springer Berlin Heidelberg.

Toworfe, G. K., Composto, R. J., Shapiro, I. M., & Ducheyne, P. (2006). Nucleation and growth of calcium phosphate on amine-, carboxyl- and hydroxyl-silane self-assembled monolayers. *Biomaterials*, *27*(4), 631-642. doi: 10.1016/j.biomaterials.2005.06.017

Uskoković, V. (2015). The Role of Hydroxyl Channel in Defining Selected Physicochemical Peculiarities Exhibited by Hydroxyapatite. *RSC advances, 5*, 36614-36633. doi: 10.1039/C4RA17180B

Uyumaz, A. N., Ozyegin, L. S., Buyukakyuz, N., Yesilbek, B., & Oktar, F. (2011). Evaluation of TCP Loaded Clinoptilolite Use as Graft Material on Rabbit Tibia. *Key Engineering Materials, 493-494*. doi: 10.4028/www.scientific.net/KEM.493-494.175

Veronese, F. M., & Pasut, G. (2005). PEGylation, successful approach to drug delivery. *Drug Discov Today, 10*(21), 1451-1458. doi: http://dx.doi.org/10.1016/S1359-6446(05)03575-0

von Marschall, Z., & Fisher, L. W. (2010). Decorin is processed by three isoforms of bone morphogenetic protein-1 (BMP1). *Biochemical and Biophysical Research Communications, 391*(3), 1374-1378. doi: http://dx.doi.org/10.1016/j.bbrc.2009.12.067

Wagoner J., A. J., & Herschler, B. A. (2011). A review of the mechanical behavior of CaP and CaP/polymer composites for applications in bone replacement and repair. *Acta Biomaterialia, 7*(1), 16-30. doi: http://dx.doi.org/10.1016/j.actbio.2010.07.012

Wallin, R., Schurgers, L. J., & Loeser, R. F. (2010). Biosynthesis of the vitamin K-dependent matrix Gla protein (MGP) in chondrocytes: a fetuin–MGP protein complex is assembled in vesicles shed from normal but not from osteoarthritic chondrocytes. *Osteoarthritis and Cartilage, 18*(8), 1096-1103. doi: http://dx.doi.org/10.1016/j.joca.2010.05.013

Wang, J., & Yu, X. (2010). Preparation, characterization and in vitro analysis of novel structured nanofibrous scaffolds for bone tissue engineering. *Acta Biomaterialia, 6*(8), 3004-3012. doi: 10.1016/j.actbio.2010.01.045

Wang, X., Nyman, J. S., Dong, X., Leng, H., & Reyes, M. (2010). Fundamental Biomechanics in Bone Tissue Engineering. *Synthesis Lectures on Tissue Engineering, 2*(1), 1-225. doi: 10.2200/S00246ED1V01Y200912TIS004

Wang, Y., Guo, G., Chen, H., Gao, X., Fan, R., Zhang, D., & Zhou, L. (2013). Preparation and characterization of polylactide/poly (ε-caprolactone)-poly (ethylene glycol)-poly (ε-caprolactone) hybrid fibers for potential application in bone tissue engineering. *Int J Nanomedicine, 9*, 1991-2003.

Wang, Y., Kim, U.-J., Blasioli, D. J., Kim, H.-J., & Kaplan, D. L. (2005). In vitro cartilage tissue engineering with 3D porous aqueous-derived silk scaffolds and mesenchymal stem cells. *Biomaterials, 26*(34), 7082-7094. doi: http://dx.doi.org/10.1016/j.biomaterials.2005.05.022

Webster, T. J., & Ahn, E. S. (2007). Nanostructured biomaterials for tissue engineering bone. *Adv Biochem Eng Biotechnol, 103*, 275-308.

Will, J., Melcher, R., Treul, C., Travitzky, N., Kneser, U., Polykandriotis, E., . . . Greil, P. (2008). Porous ceramic bone scaffolds for vascularized bone tissue regeneration. *Journal of Materials Science: Materials in Medicine, 19*(8), 2781-2790.

Woo, K. M., Chen, V. J., & Ma, P. X. (2003). Nano-fibrous scaffolding architecture selectively enhances protein adsorption contributing to cell attachment. *Journal of Biomedical Materials Research Part A, 67*(2), 531-537.

Wopenka, B., & Pasteris, J. D. (2005). A mineralogical perspective on the apatite in bone. *Materials Science and Engineering: C, 25*(2), 131-143. doi: 10.1016/j.msec.2005.01.008

Yang, W. W., & Pierstorff, E. (2012). Reservoir-based polymer drug delivery systems. *J Lab Autom, 17*(1), 50-58. doi: 10.1177/2211068211428189

Yu, L., Gong, J., Zeng, C., & Zhang, L. (2013). Preparation of zeolite-A/chitosan hybrid composites and their bioactivities and antimicrobial activities. *Materials Science and Engineering: C, 33*(7), 3652-3660. doi: 10.1016/j.msec.2013.04.055

Zaiss, S., Brown, T., Reichert, J., & Berner, A. (2016). Poly(ε-caprolactone) Scaffolds Fabricated by Melt Electrospinning for Bone Tissue Engineering. *Materials, 9*(4), 232.

Zhang, J., Yang, S.-G., Ding, J.-X., & Li, Z.-M. (2016). Tailor-made poly(l-lactide)/poly(lactide-co-glycolide)/hydroxyapatite composite scaffolds prepared via high-pressure compression molding/salt leaching. *RSC advances, 6*(53), 47418-47426. doi: 10.1039/C6RA06906A

Zhao, J., Guo, L. Y., Yang, X. B., & Weng, J. (2008). Preparation of bioactive porous HA/PCL composite scaffolds. *Applied Surface Science, 255*(5, Part 2), 2942-2946. doi: http://dx.doi.org/10.1016/j.apsusc.2008.08.056

Zhao, J., Liu, Y., Sun, W.-b., & Zhang, H. (2011). Amorphous calcium phosphate and its application in dentistry. *Chemistry Central Journal, 5*, 40-40. doi: 10.1186/1752-153X-5-40

Zhou, S., Deng, X., & Yang, H. (2003). Biodegradable poly (ε-caprolactone)-poly (ethylene glycol) block copolymers: characterization and their use as drug carriers for a controlled delivery system. *Biomaterials, 24*(20), 3563-3570.

Zhu, W., Masood, F., O'Brien, J., & Zhang, L. G. (2015). Highly aligned nanocomposite scaffolds by electrospinning and electrospraying for neural tissue regeneration. *Nanomedicine: Nanotechnology, Biology and Medicine, 11*(3), 693-704. doi: http://dx.doi.org/10.1016/j.nano.2014.12.001

APPENDIX A

CALIBRATION CURVE FOR PROTEIN ADSORPTION STUDIES

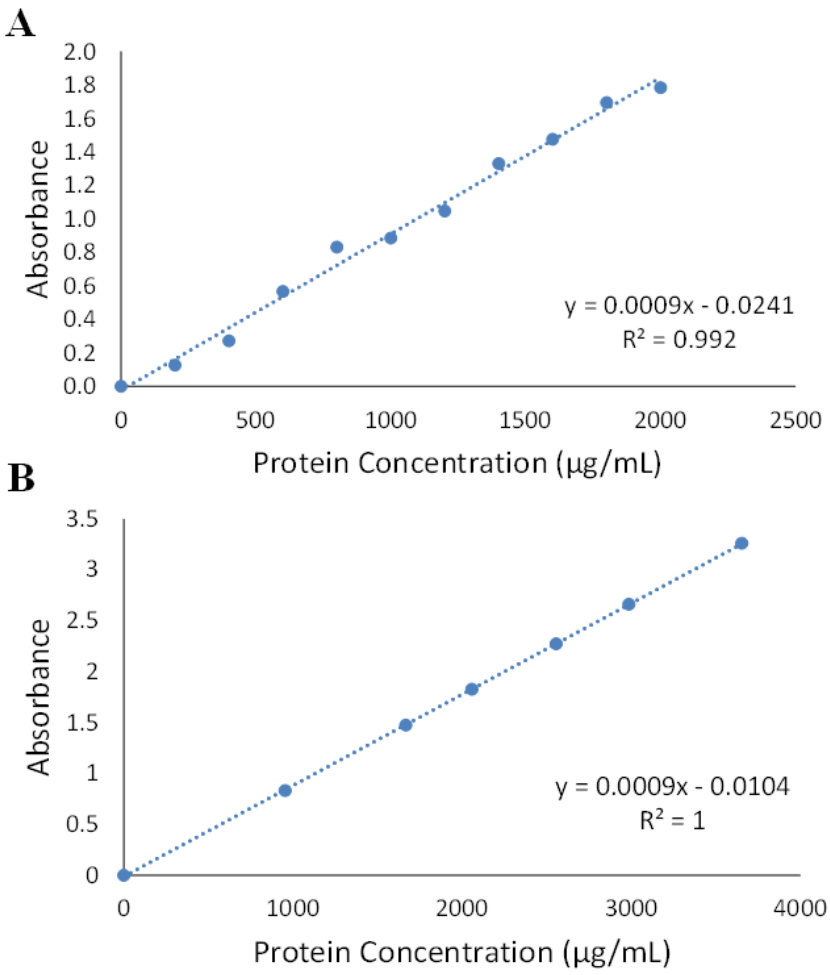

Figure 23. Calibration curves for MicroBCA assay constructed using different concentrations of BSA for the clinoptilolite protein adsorption study (A) and for scaffold protein adsorption study (B) (n=3 for both studies).

APPENDIX B

CALIBRATION CURVES FOR ALP AND OSP

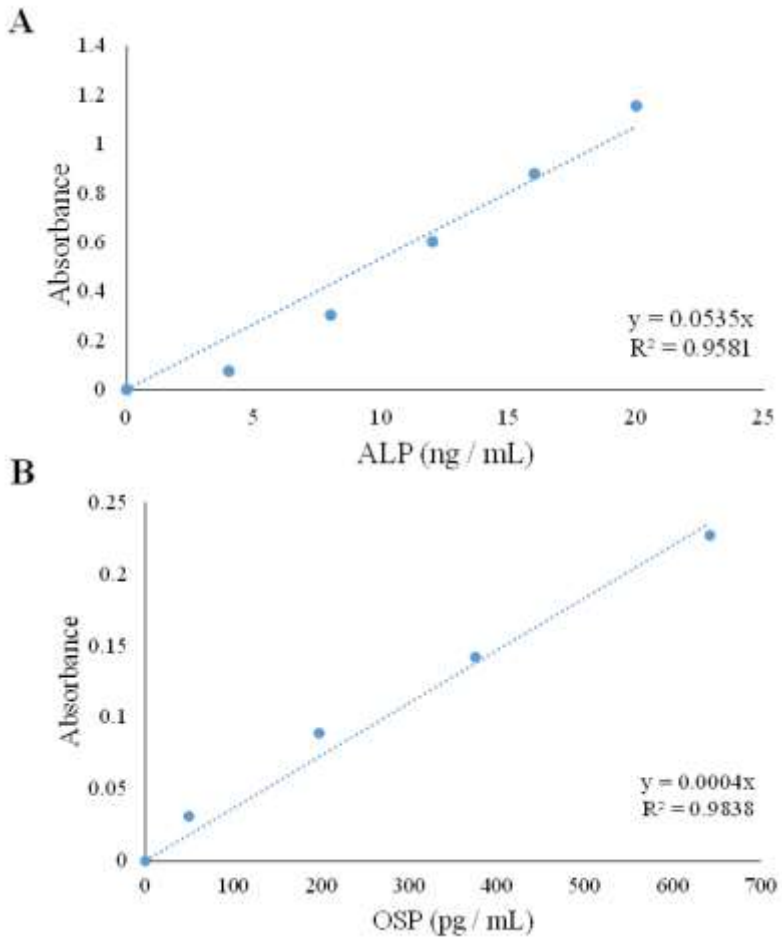

Figure 24. Calibration curves for ALP assay constructed with para-nitrophenol as standard (supplier's protocol) (A) and for OSP using kit's standards (B) (n=2 for both studies).

APPENDIX C

CALIBRATION CURVE FOR DETERMINATION OF INTRACELLULAR CALCIUM

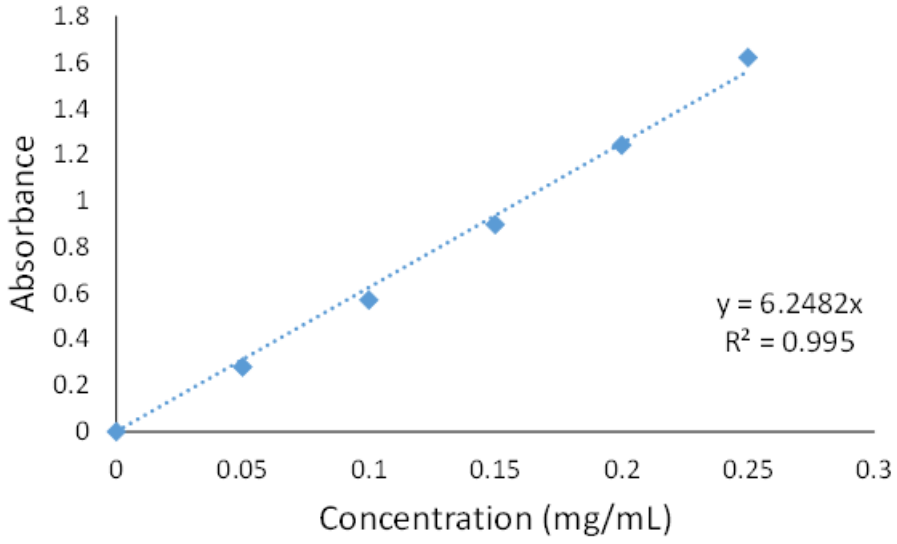

Figure 25. Calibration curve of calcium using various $CaCl_2$ concentrations as standard (n=5).

APPENDIX D

CALCULATION of M_n of PCEC

Calculation of M_n from ^1H NMR results where (1) shows initial feed molar ratio and (2) displays the final, experimental result:

$$\frac{[CL]}{[EG]} = \frac{\frac{144\ g/mol}{6\ g}}{\frac{44\ g/mol}{0.25\ g/mol}} = 9.25/1 \quad (1)$$

$$\frac{[CL]}{[EG]} = \frac{I_a/_4}{I_a/_4 + I_g/_4} = \frac{10.7}{10.7+2.09} = 0.84 \quad (2)$$

where 84% of the copolymer is formed by PCL homosequences. Then,

$$\frac{[CL]}{[EG]} = \frac{0.84}{0.16} = 5.25/1 \quad (3)$$

Finally,

$$\overline{DP}_{PEG} = \frac{M_{n^{PEG}}}{44} = \frac{4000}{44} = 90.9 = 91 \quad (4)$$

$$\overline{DP}_{PCL} = \frac{M_{n^{PEG}}}{44} * \frac{[CL]}{[EG]} = 91 * 5.25 = 477.75 = 478 \quad (5)$$

$$M_n = M_{n^{PEG}} + 114 * \overline{DP}_{PCL} = 4000 + 114 * 478 = 58492 = 58\ kDa \quad (6)$$

APPENDIX E

TNE BUFFER AND HOECHST DNA DYE PREPARATION

Steps for TNE Buffer Preparation

T: Tris-base buffer – to keep pH of the system close to 7.4 and enable DNA extraction

N: NaCl. It brings about dehydration of DNA from water to extract DNA easily.

E: EDTA – Chelates any free metal ion to prevent DNA damage

Table 8. TNE Buffer components required for 1L, 10X preparation

Weight (g)	Name
12.11	Trishydroxymethyl aminomethane (Tris-base)
3.72	EDTA disodium salt dihydrate
116.89	Sodium chloride
7.4	Final pH

Steps for Hoechst 33258 Dye Preparation

1. Dissolve Hoechst (1 mg/mL) in deionized water to preparare stock and prepare TNE buffer. Filter both solutions through 0.45 um filter
2. 20 μL from Hoechst stock and 100 mL 1X TNE Buffer (5000X folds dilution) is employed to prepare 2X stain solution for staining
3. Add samples as:
    a. Cell lysis by ALP lysis buffer is conducted

b. Collect aliquot of 250 µL and mix with 750 µL 1X TNE buffer

c. Add 1000 µL Hoechst stain solution to get 1:1 (v/v) ratio and obtain 1X stain solution

4. Read the samples in quartz cuvettes in fluorometer with UV attachment

APPENDIX F

CALIBRATION CURVE FOR DETERMINATION OF DNA CONTENT

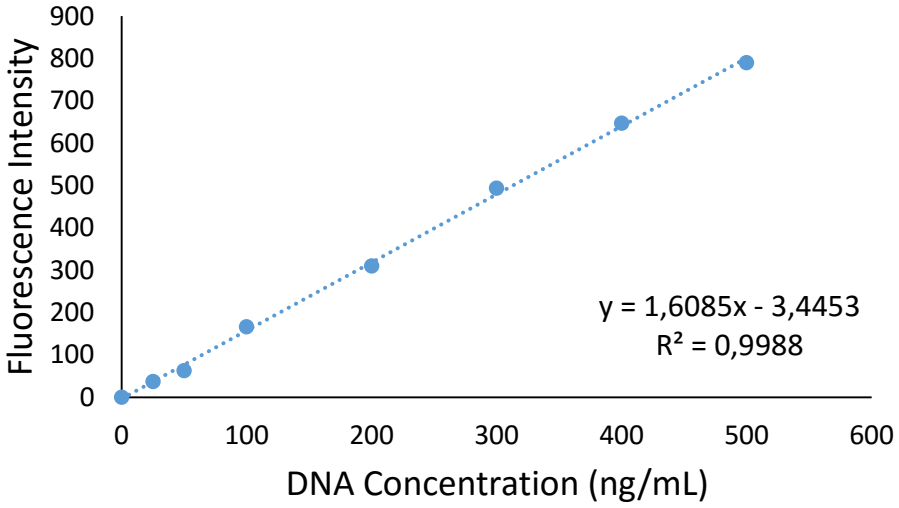

Figure 26. Calibration curve of DNA constructed with different concentrations of calf thymus DNA as standard for the determination of total DNA content in cell lysates in ALP assay (n=3).